Chem Soc Rev

This article was published as part of the

2008 Chemistry at Surfaces issue

Reviewing the latest developments in surface science

All authors contributed to this issue in honour of the 2007 Nobel Prize winner
Professor Gerhard Ertl

Please take a look at the issue 10 table of contents to access the other reviews

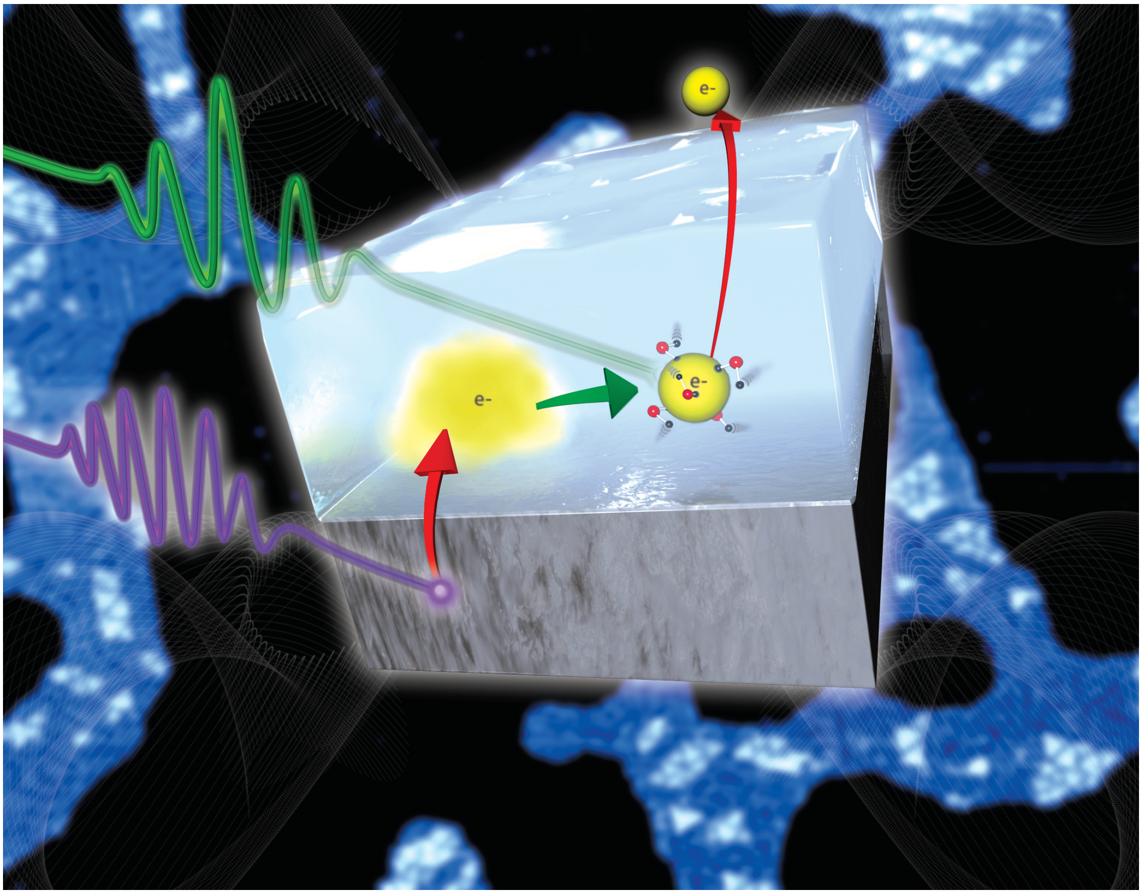

Chemical reactions on rutile $TiO_2(110)$†

Chi Lun Pang,[a] Robert Lindsay[b] and Geoff Thornton*[a]

Received 11th August 2008
First published as an Advance Article on the web 4th September 2008
DOI: 10.1039/b719085a

Understanding the surface chemistry of TiO_2 is key to the development and optimisation of many technologies, such as solar power, catalysis, gas sensing, medical implantation, and corrosion protection. In order to address this, considerable research effort has been directed at model single crystal surfaces of TiO_2. Particular attention has been given to the rutile $TiO_2(110)$ surface because it is the most stable face of TiO_2. In this *critical review*, we discuss the chemical reactivity of $TiO_2(110)$, focusing in detail on four molecules/classes of molecules. The selected molecules are water, oxygen, carboxylic acids, and alcohols—all of which have importance not only to industry but also in nature (173 references).

1. Introduction

Given the importance of TiO_2 surface chemistry in a variety of technologies,[1–7] such as solar cells, catalysis, gas sensing, medical implantation, and corrosion protection, it is hardly surprising that there is a tremendous drive to probe and enhance the chemical reactivity of this material. Currently, research in this field is wide-ranging, with activity extending from synthesis of novel titania based structures (*e.g.* nanotubes[8]) to fundamental work aiming to comprehend surface chemistry at the atomic scale (see, for example, ref. 9). This latter effort is typically concerned with studies of model low Miller index single crystal surfaces under ultra-high vacuum (UHV) conditions, in order to simplify the problem. Here, to celebrate Gehard Ertl's Nobel Chemistry Prize "for his studies of chemical processes on solid surfaces",[10] we review such fundamental studies of chemical processes on TiO_2, focusing on the rutile $TiO_2(110)$ surface.

To date, rutile $TiO_2(110)$ is the most studied single crystal TiO_2 surface. Indeed, its 1×1 termination has emerged as *the* prototypical metal oxide surface for fundamental studies. It serves as a playground for researchers exploring a wide variety of important topics, including surface chemistry at both regular terrace sites and defects. A number of factors have contributed to this surface's pre-eminence for such work, including the ready availability of high quality crystals, its significant electrical conductivity following annealing in vacuum, and the relative simplicity of the geometric structure of the 1×1 phase.

In this *critical review*, we are not only concerned with the chemistry of $TiO_2(110)1\times1$, but also that of the reconstructed 1×2 phase(s). We concentrate on the reactivity of these surfaces with a number of technologically important molecules, namely H_2O, O_2, $R(COOH)_n$, and $R(OH)_n$, updating information provided in the seminal review of the surface science of TiO_2 by Diebold.[11] Prior to discussing the reactivity of $TiO_2(110)$ with the various molecules, we present pertinent details of the structure of the clean 1×1 and 1×2 surfaces.

2. Clean surface

Key to the value of surface chemistry studies on model substrates is a detailed knowledge of clean surface structure. Without this information, mechanistic interpretation of reactions can at best be speculative, at worst simply incorrect. For $TiO_2(110)$, fortunately, many structural aspects are well characterised, in particular for the 1×1 phase.

---

[a] *London Centre for Nanotechnology and Department of Chemistry, University College London, London, UK WC1H 0AJ*
[b] *Corrosion and Protection Centre, School of Materials, The University of Manchester, PO Box 88, Manchester, UK M60 1QD*

† Part of a thematic issue covering reactions at surfaces in honour of the 2007 Nobel Prize winner Professor Gerhard Ertl.

Chi Lun Pang received his BSc in Chemistry from the University of Southampton before obtaining MRes and PhD qualifications at the University of Manchester. He held research posts at the University of Manchester and the University of Reading before taking up a JSPS Research Fellowship at Kobe University. He is currently working as a Senior Experimental Officer in Geoff Thornton's group in London.

Robert Lindsay received a BSc in Chemistry from the University of Bristol, and a PhD from the University of Liverpool. He has had appointments at a number of research institutions, including the Fritz Haber Institut (Berlin), Cambridge University, and the CSIC Institute of Materials in Barcelona. Currently, he is a Lecturer in Corrosion Science and Engineering at the University of Manchester.

Geoff Thornton is Professor of Physical Chemistry at University College London and a resident of the London Centre for Nanotechnology. He received a DPhil from the University of Oxford before taking up an 1851 Research Fellowship at Oxford and subsequently UC Berkeley. He was appointed to a lectureship at Manchester University in 1979 where he remained until 2003 when he moved to UCL. He was Assistant Director of the IRC in Surface Science between 1988 and 1998.

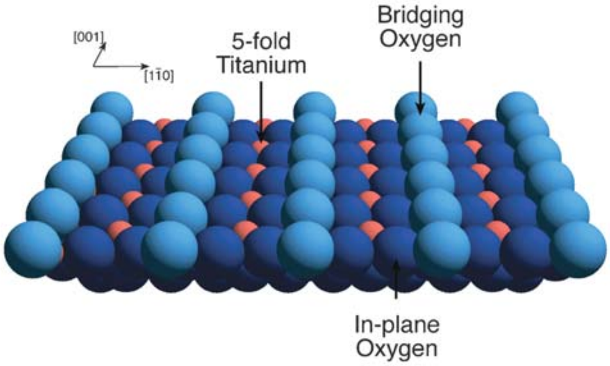

Fig. 1 A pseudo-space-filling model of the ideal bulk-terminated $TiO_2(110)1\times1$ surface.

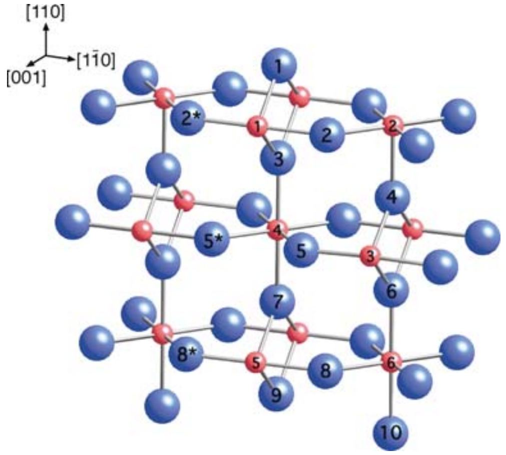

Fig. 2 Ball and stick model of $TiO_2(110)1\times1$. Larger (smaller) spheres are oxygen (titanium) ions. The numerical labelling of the atoms is employed in Table 1 for identification purposes. Symmetry paired atoms are denoted as 2*, 5*, and 8*.

Fig. 1 displays a pseudo-space-filling model of the ideal bulk-terminated $TiO_2(110)1\times1$ surface, consisting of so-called bridging oxygens (O_b), 5-fold titaniums (Ti_{5c}), and in-plane oxygens at the solid–vacuum interface. The presence of this structure, following typical UHV surface preparation comprising inert gas ion bombardment and annealing cycles, has been confirmed experimentally using various quantitative probes of surface crystallography.[12–18] The most cited of these studies to date is a surface X-ray diffraction (SXRD) study published by Charlton *et al.* in 1997.[12] Given that the displacements of the 11 topmost oxygen and titanium atoms (Ti(1)–Ti(4) and O(1)–O(7) in Fig. 2) were determined with significant precision, this structure has been considered a benchmark by many researchers. However, there has been debate about the complete accuracy of the optimised structure, with the bridging oxygen atom (O(1) in Fig. 2) being of primary concern. This situation has motivated a recent re-examination of the relaxation of the $TiO_2(110)1\times1$ surface, employing a number of quantitative structural probes,[15–18] including a more recent SXRD study.[18]

Table 1 lists the atomic displacements corresponding to the optimised structures emerging from the various recent experimental studies,[15–18] along with those from Charlton *et al.*'s work.[12] It is clear from this table that none of the latter work replicates the relaxation of the bridging oxygen (O(1)) towards the bulk determined in ref. 12, rather all find that the oxygen

Table 1 Atomic displacements away from the bulk-terminated structure of $TiO_2(110)1\times1$ from Charlton *et al.*'s SXRD study,[12] and more recent experimental work.[15–18] Fig. 2 provides a key to the identity of the atoms. A negative value indicates that the atom moves towards the bulk for a displacement perpendicular to the surface plane, and in the [1$\bar{1}$0] direction for a lateral displacement

	Displacement/Å				
Atom	SXRD (Charlton *et al.*) Ref. 12	LEED-IV Ref. 15	MEIS Ref. 16	PhD Ref. 17	SXRD Ref. 18
Ti(1)	0.12 ± 0.05	0.25 ± 0.03	0.19 ± 0.07	0.19 −0.15/+0.10	0.25 ± 0.01
Ti(2)	−0.16 ± 0.05	−0.19 ± 0.03	−0.09 ± 0.09	−0.26 ± 0.08	−0.11 ± 0.01
Ti(3)	−0.09 ± 0.04	−0.09 ± 0.07	−0.09 ± 0.09	−0.21 −0.40/+0.15	−0.08 ± 0.01
Ti(4)	0.07 ± 0.04	0.14 ± 0.05	−0.06 ± 0.06	0.15 −0.20/+0.15	0.19 ± 0.01
O(1)	−0.27 ± 0.08	0.10 ± 0.05	0.13 ± 0.16	0.17 ± 0.15	0.10 ± 0.04
O(2) [110]	0.05 ± 0.05	0.27 ± 0.08	0.05[a]	0.00 −0.40/+0.15	0.17 ± 0.03
O(2) [1$\bar{1}$0]	−0.16 ± 0.08	−0.17 ± 0.15	0.00[a]	−0.05 ± 0.15	0.01 ± 0.05
O(3)	0.05 ± 0.08	0.06 ± 0.10	0.10 ± 0.13	0.15 ± 0.15	0.07 ± 0.04
O(4)	0.00 ± 0.08	0.00 ± 0.08	—	−0.03 ± 0.08	0.00 ± 0.03
O(5) [110]	0.02 ± 0.06	0.06 ± 0.12	—	—	0.04 ± 0.03
O(5) [1$\bar{1}$0]	−0.07 ± 0.06	−0.07 ± 0.18	—	—	0.05 ± 0.05
O(6)	−0.09 ± 0.08	0.00 ± 0.17	—	—	0.01 ± 0.04
O(7)	−0.12 ± 0.07	0.01 ± 0.13	—	—	0.01 ± 0.04
O(8) [110]	—	—	—	—	0.01 ± 0.03
O(8) [1$\bar{1}$0]	—	—	—	—	−0.03 ± 0.05
Ti(5)	—	—	0.00 ± 0.07		0.08 ± 0.01
Ti(6)	—	—	−0.02 ± 0.08	—	−0.04 ± 0.01
O(9)	—	—	—	—	0.02 ± 0.04
O(10)	—	—	—	—	−0.02 ± 0.04

[a] No error estimates are given in ref. 16 for these parameters, due to their strong coupling.

shifts away from the bulk. Furthermore, the displacements of almost all other optimised atoms are quantitatively similar across all of these recent measurements. Agreement is most impressive for the quantitative low energy electron diffraction (LEED-IV)[15] and the latest SXRD[18] experiments, as many of the atomic displacements have been determined with high precision (the error bars associated with the medium energy ion scattering (MEIS) and photoelectron diffraction (PhD) structures are typically somewhat larger).

Comparing experiment with first-principles calculations of the geometric structure of $TiO_2(110)1\times1$, these two strands of effort are apparently beginning to converge. In particular, no recent theoretical studies predict that the bridging oxygen (O(1)) relaxes significantly towards the bulk; it either maintains its ideal bulk-terminated position,[19,20] or shifts away from the bulk.[21–23] However, exact atomic coordinates are dependent on the theoretical approach adopted, and further work is required to establish a fully reliable, quantitative theoretical description of the atomic geometry of $TiO_2(110)1\times1$.

Scanning probe microscopy (SPM) images of $TiO_2(110)1\times1$ are also consistent with the structure displayed in Fig. 1 and 2 (see, for example, refs. 11, 24–28), although no further insight into the coordinates of surface atoms is gained. The real value of these probes is the visualisation of surface imperfections, such as step edges, which are not normally accessible to spatially integrating diffraction/scattering techniques. Of particular importance, as regards surface chemistry, are bridging oxygen vacancies (O_b-vacs), which are the primary point defects on this surface. Following standard substrate preparation in UHV, several percent of bridging oxygen atoms are missing;[28] the concentration of O_b-vacs can be controlled through variation of the annealing temperature.[29] Given sufficient lateral resolution and appropriate tip condition, these thermally induced vacancies can be imaged by both scanning tunnelling spectroscopy (STM), and non-contact atomic force microscopy (NC-AFM). Almost all published STM images show missing O_b as bright protrusions on dark rows (see Fig. 3), the bright rows of the perfect terraces being due to Ti_{5c} rather than O_b.[24,25] STM images can also be obtained in which dark spots appear on bright rows but because such images are not well understood they will not be discussed further in this review.[26] In both these cases and in all other STM images presented in this review, positive tunnelling is used so that electrons tunnel from filled tip states into empty states of the sample. In NC-AFM, the O_b-vacs are usually observed as dark depressions on bright rows, which in this case are the O_b rows.[27]

Besides locally perturbing the geometry of $TiO_2(110)1\times1$, O_b-vacs give rise to an occupied band gap state (BGS), which from resonant photoemission is known to have primarily Ti 3d character.[30–32] This BGS can be directly observed spectroscopically,[30–36] as demonstrated by Fig. 4, which displays valence band photoelectron spectroscopy (PES) spectra from (i) defect free $TiO_2(110)1\times1$, and (ii) $TiO_2(110)1\times1$ decorated with O_b-vacs. It is also generally accepted that the presence of this defect state is reflected in Ti 2p core level PES by the appearance of a low binding energy shoulder, shifted by ~1.7 eV from the primary peak. Typically, these features are nominally assigned to Ti^{3+} and Ti^{4+}, respectively, although it is clear from both experiment and theoretical modelling that bonding in TiO_2 has significant covalent character.[23,30,31]

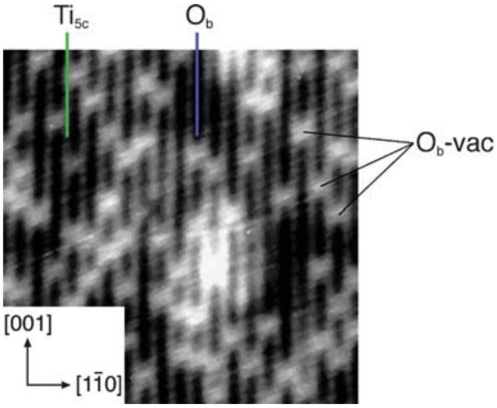

Fig. 3 (135 Å)^2 STM image of $TiO_2(110)1\times1$. The bright rows correspond to Ti_{5c} sites and the dark rows to O_b sites. O_b-vacs appear on the dark rows as bright spots, three of which are labelled.

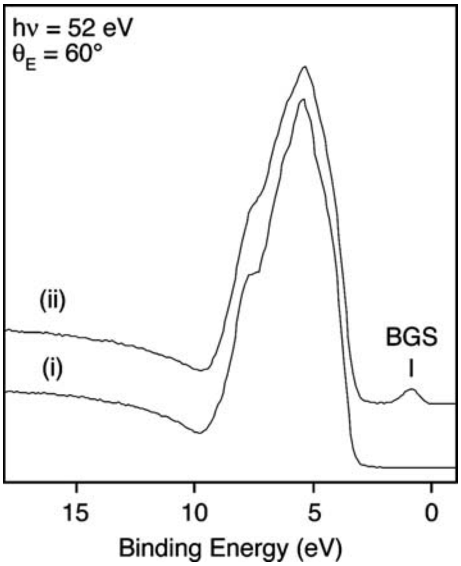

Fig. 4 Valence band PES spectra from (i) defect free $TiO_2(110)1\times1$ and (ii) $TiO_2(110)1\times1$ decorated with O_b-vacs. The BGS due to O_b-vacs is indicated.

Very recently, the spatial distribution of the electronic charge associated with the O_b-vac induced BGS has been probed by scanned-angle mode PhD at the Ti 2p–Ti 3d resonance.[37] It is concluded that the charge is distributed across several Ti atoms, both surface and subsurface, with the majority being located on a second layer Ti (Ti(3) in Fig. 2). Only a small amount of the charge is possessed by surface layer titaniums (Ti(1) and Ti(2) in Fig. 2).

In addition to surface reduction, annealing a $TiO_2(110)$ sample in UHV leads to substoichiometry in the bulk, which is indicated by changes in sample colour.[38] A pristine stoichiometric TiO_2 single crystal sample is transparent, but with increasing bulk reduction becomes green-blue, light/dark blue, and finally dark blue-black. For considerably reduced (darker) crystals, the (110) surface also reconstructs, usually to either a simple 1×2 or a cross-linked 1×2 phase.[39–54]

Various models for the geometric structure of simple $TiO_2(110)1\times2$ have been reported in the literature. Initially, on the basis of Auger electron spectroscopy (AES), a simple missing-row model was suggested, formed by the loss of alternate rows of bridging oxygen from the bulk terminated 1×1 surface.[39] On the basis of high resolution SPM images, this model has fallen out of favour to be replaced by models involving added rows. Onishi and Iwasawa have proposed that these added rows have Ti_2O_3 stoichiometry, although not the structure found in bulk Ti_2O_3 crystals.[40,41] Pang *et al.* have hypothesised a contrasting model, comprising Ti_3O_5 added rows, which is supported by theoretical simulations of their STM images.[42,43] Another model, developed by Park *et al.*, involves added Ti_2O rows.[44]

Recently, Blanco-Rey *et al.* have removed the uncertainty surrounding the identity of the simple 1×2 added rows, through the employment of LEED-IV.[45,46] They have demonstrated that the added rows have the Ti_2O_3 architecture suggested by Onishi and Iwasawa.[40,41] Fig. 5 shows a ball and stick model of the structure, and Table 2 lists atomic coordinates of optimised atoms. This geometry is supported by electron stimulated desorption ion angular distribution (ESDIAD) data,[47] ion scattering measurements,[48] and *ab initio* calculations.[49,50]

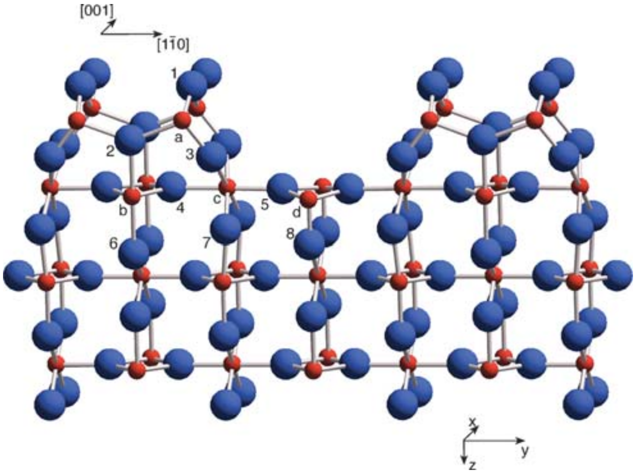

Fig. 5 Ball and stick model of the *simple* $TiO_2(110)1\times2$ reconstruction with added Ti_2O_3 rows. Larger (smaller) spheres are oxygen (titanium) ions. The labelling of the atoms is employed in Table 2 for identification purposes.

Table 2 Optimised atomic coordinates obtained from Blanco-Rey *et al.*'s LEED-IV study of *simple* $TiO_2(110)(1\times2)$.[45] Fig. 5 provides a key to the identity of the atoms, and the *x*, *y*, *z* directions

	Coordinates/Å		
Atom	*x*	*y*	*z*
Ti(a)	1.48	1.77	−5.99 ± 0.03
Ti(b)	1.48	0.00	−3.14 ± 0.07
Ti(c)	0.00	3.28	−3.27 ± 0.06
Ti(d)	1.48	6.49	−3.08 ± 0.05
O(1)	0.00	1.99	−7.16 ± 0.24
O(2)	1.48	0.00	−5.23 ± 0.07
O(3)	1.48	3.07	−4.60 ± 0.11
O(4)	0.00	1.25	−3.21 ± 0.12
O(5)	0.00	5.22	−3.54 ± 0.06
O(6)	1.48	0.00	−1.30 ± 0.22
O(7)	1.48	3.28	−2.03 ± 0.22
O(8)	1.48	6.49	−1.31 ± 0.12

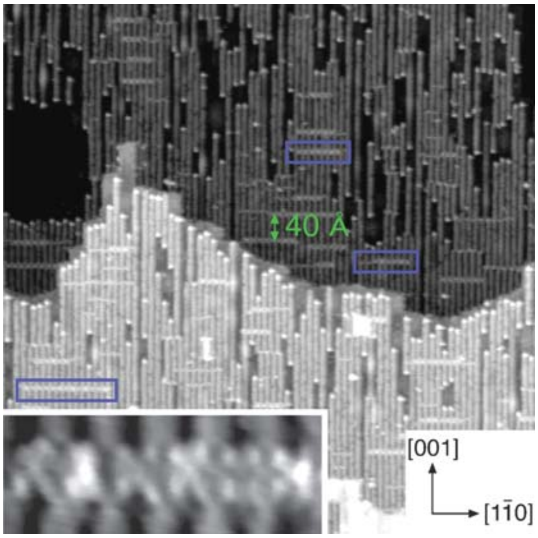

Fig. 6 (1060 Å)^2 STM image of x-linked $TiO_2(110)1\times2$. Some x-links are marked with blue rectangles. The separation between a pair of x-links is indicated. The inset shows an 80 Å × 30 Å STM image of a similar surface, highlighting the cross shapes of the links.

Further STM studies, by Bennett *et al.*, suggest that the exact nature of the $TiO_2(110)$ reconstruction is dependent on the extent of the bulk reduction of the TiO_2 sample.[51] They have found that more stoichiometric samples (medium blue) exhibit the simple 1×2 reconstruction, but that well-reduced substrates (blue-black) display an x-linked 1×2 structure. In addition to added rows, STM images (see Fig. 6) of this latter phase show the presence of cross shaped structures connecting neighbouring 1×2 rows, very roughly one every 12 unit cells in the [001] direction. Bennett *et al.* also conclude that the structure of the added rows is different on simple 1×2 and x-linked 1×2 surfaces. They assign the simple 1×2 added-rows to Onishi and Iwasawa's Ti_2O_3 model,[40,41] whereas they suggest that x-linked 1×2 added rows are consistent with a slightly modified version of Pang *et al.*'s model,[42,43] in which an additional oxygen is incorporated into the added rows *i.e.* Ti_3O_5 becomes Ti_3O_6. However, this assignment of the x-linked added rows to Ti_3O_6 is disputed. For instance, it is claimed in ref. 52 that they have the Onishi and Iwasawa Ti_2O_3 structure. Unpublished LEED-IV and SXRD data[53] also support a Ti_2O_3 stoichiometry for the x-linked added rows.

3. Water

TiO_2 photocatalyses the splitting of water, and it is this photoactivity which underpins the use of TiO_2 in green technology such as self-cleaning windows, air/water purification devices, and novel solar cells. Moreover, water is present in virtually all conceivable technological applications of TiO_2. As such, the interaction of water with TiO_2 surfaces is a crucial area of research.

Here, we examine the dissociation of water in O$_b$-vacs, the properties of water layers, and $TiO_2(110)$ under ambient water pressures. Given that the enormous body of work discussing water adsorption on $TiO_2(110)$ has been extensively reviewed by Henderson in 2002[55] and summarised again in Diebold's review,[11] we will introduce earlier work only briefly and focus on the significant advances made in this area in the past few years. As there are very few studies of water on the 1×2 terminations,[56] only work on the 1×1 surface will be considered in this section.

Throughout this review, the coverage of molecules adsorbed on $TiO_2(110)$ will be given in monolayers (ML), where 1 ML corresponds to one adsorbate per primitive surface unit cell. Gas and vapour exposures will be given in Langmuirs (L) where $1\ L = 1.33 \times 10^{-6}$ mbar s.

3.1 Water dissociation

Nearly all experimental studies of water adsorption on $TiO_2(110)1\times1$ indicate that water dissociates only at O$_b$-vacs, as shown in the reaction scheme in Fig. 7. Water fills the vacancy and one of the hydrogen atoms splits off leaving a bridging hydroxyl group (OH$_b$) at the vacancy. The hydrogen atom sits on a nearby bridging O atom, forming another OH$_b$ species.

Temperature programmed desorption (TPD) spectra of water on $TiO_2(110)$ give peaks at ~163 K, ~175 K, ~265 K, and ~490 K, as shown in Fig. 8.[57–60] For now, we will discuss only the two higher temperature peaks.

When the surface was isotopically enriched with ^{18}O before exposure to $H_2{}^{16}O$, $H_2{}^{18}O$ was preferentially desorbed at ~490 K.[59] This not only shows that the ~490 K peak must arise from the recombination of dissociated water, it also indicates that the hydrogen atoms of OH$_b$ can diffuse to other O$_b$ sites. As the coverage of water (~0.09 ML) desorbed in the ~490 K peak matches expectations of the O$_b$-vac concentration,[57] it was concluded that water dissociates at the O$_b$-vacs.[60] In contrast, only $H_2{}^{16}O$ desorbed at ~265 K, suggestive of molecular adsorption.

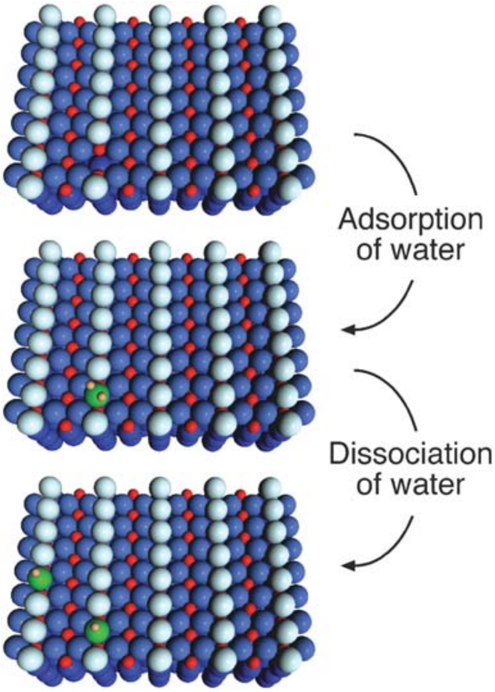

Fig. 7 Schematic depictions of water dissociation on $TiO_2(110)$. Blue and red spheres denote lattice O and Ti, respectively. The light blue spheres are O$_b$ atoms, which lie in the [001] azimuth of the substrate. Parallel Ti rows that lie between the O$_b$ rows are Ti$_{5c}$ atoms. Green spheres indicate O atoms bonded to H atoms which are shaded pink.

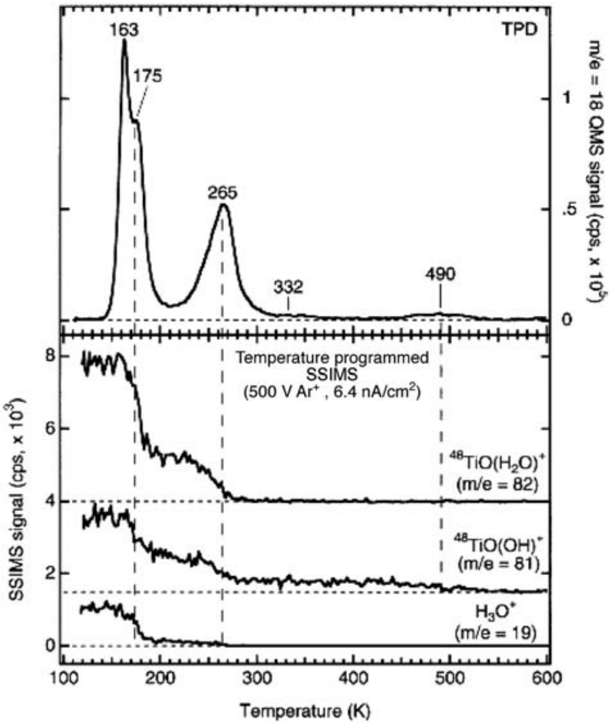

Fig. 8 TPD (upper panel) and temperature programmed SSIMS (lower panel) spectra from a multilayer exposure of H_2O adsorbed on $TiO_2(110)$ at 110–118 K. Some spectra are displaced vertically for clarity. Background levels in TPD and zero signal levels in SSIMS are indicated by horizontal dashed lines. Modified with permission from ref. 60.

These peaks were further identified with molecular and dissociative adsorption using static secondary ion mass spectrometry (SSIMS), as shown in Fig. 8. $TiO(H_2O)^+$ and $TiO(OH)^+$ peaks were monitored as a function of anneal temperature following exposure to water. The $TiO(H_2O)^+$ signal falls to zero at ~265 K whereas the $TiO(OH)^+$ signal attenuates at ~490 K.[60]

As discussed in section 2, spectroscopic probes detect a BGS ~0.8–0.9 eV below E_F which is associated with O$_b$-vacs.[30–32] Resonant PES spectra show that water exposure even up to 100 L (at ~300 K) does not attenuate the defect state, indicating that *electronically* the O$_b$-vacs are not healed by water,[33] a conclusion also formed on the basis of electron energy loss (EELS) data.[34] In line with these observations, theoretical calculations have recently detected the presence of BGS for both O$_b$-vacs and OH$_b$.[61]

Brookes *et al.*[62] used STM at a range of temperatures in order to observe this water dissociation, as shown in Fig. 9. The key result was a switch from bright spots being adsorbed on the bright rows at ≤200 K to bright spots appearing

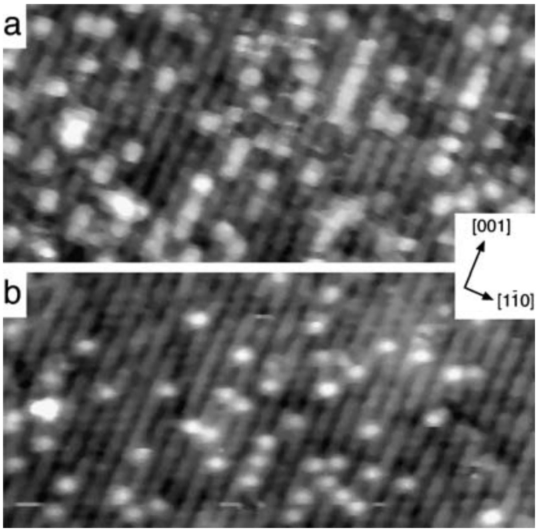

Fig. 9 175 Å × 90 Å STM images of $TiO_2(110)$ exposed to 3.5 L H_2O at 150 K, and consecutively heated to the measurement temperatures of (a) 195 K and (b) 290 K. Modified from ref. 62 with permission.

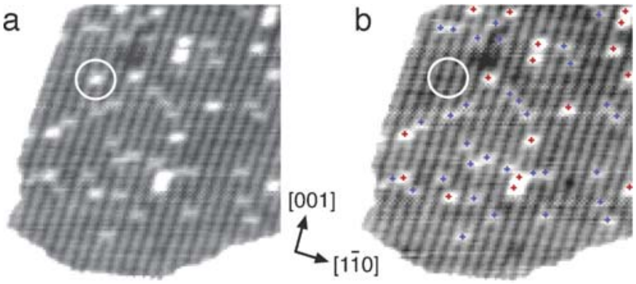

Fig. 10 Sequential (150 Å)^2 STM images of as-prepared $TiO_2(110)$. The densities of A_b and A_d defects are ~1.5% and ~3.0%, respectively. (a) Before a voltage pulse and (b) after the voltage pulse. The voltage pulse (+3 V, 0.35 nA, 300 ms) was applied to the A_b defect circled in (a). In (b), A_b and A_d defects are marked with red and blue crosses, respectively, and the pulsed A_b defect is missing. Modified from ref. 28 with permission.

between bright rows at ~290 K. The bright spots at ≤200 K were assigned to molecular water adsorbed on Ti_{5c} sites. As the concentration of the bright spots at ~290 K is about ~0.08 ML, Brookes *et al.*[62] infer that they represent OH_b formed from water dissociated in O_b-vacs.

By imaging the reaction dynamically, STM has the power to directly follow the dissociation of water in O_b-vacs. However, an obvious prerequisite is that O_b-vacs must be unambiguously identified in STM images. As discussed in section 2, STM images of $TiO_2(110)$ are generally thought to show O_b-vacs as bright spots on dark O_b rows.[24] However, based on STM imaging and electron stimulated desorption (ESD) experiments, Suzuki *et al.*[63] suggested that these bright spots (also known as type-A defects) originate from OH_b; the source of hydrogen being residual water vapour or H_2 in the vacuum chamber. Schaub *et al.*[64] partially resolved this issue by showing the presence of two kinds of type-A defects (see Fig. 10). The brighter (A_b) defects were assigned to O_b-vacs and the darker (A_d) defects to OH_b.

The evidence for this assignment was two-fold. First, their DFT simulations of STM images suggest that O_b-vacs should be brighter than OH_b. Second, the concentration of type-A defects after exposing $TiO_2(110)$ to water was counted to be about twice the number of A_b defects before exposure, consistent with water dissociation in O_b-vacs forming two OH_b species.

Evidence accumulated over the past few years, however,[28,65–69] reverses the assignment of type-A defects by Schaub *et al.*[64] One of the keys to distinguishing OH_b from O_b-vacs was suggested by studies in which the STM tip was scanned over the $TiO_2(110)$ surface at a raised voltage of +3 V. Type-A defects were removed from the surface and interpreted as tip-induced refilling of O_b-vacs by Diebold *et al.*[70] and as tip-induced removal of hydrogen from OH_b by Suzuki *et al.*[63]

Bikondoa *et al.*[28,65] removed *individual* type-A defects with electrical pulses at *ca.* +3 V, as shown in Fig. 10. Crucially, only A_b defects could be removed in this way and this was used as a means to distinguish the two types of defects. A_b defects were removed by scanning at a raised bias of +3 V, creating an A_b defect-free region (the 'clean-off area') before exposing to water, as shown in Fig. 11. If the A_b defects are O_b-vacs as suggested by Schaub *et al.*,[64] then exposure to water should have little effect in the clean-off area as there would be no O_b-vacs to react with. On the other hand, if the A_d defects are O_b-vacs, then exposure of the surface to water should replenish the A_b defects in the clean-off area, due to water molecules dissociating in the O_b-vacs.

It turned out that exposure of the surface to water led to the replenishment of A_b defects in the clean-off area (Fig. 11c), so that A_b defects were assigned to OH_b and A_d defects to O_b-vacs. This also means that the *ca.* +3 V scans and tip pulses desorbed hydrogen from the OH_b groups. Whilst the mechanism for this hydrogen desorption is as yet unknown, it may be related to an empty state identified by Onda *et al.*[71] using two-photon photoemission (2PP) spectroscopy and assigned as a 'wet electron state'; a wet electron state being a partially hydrated state. This state was found ~2.4 eV above E_F, maximising when OH_b coexists with 1 ML of molecular water.

Returning to Fig. 11c: because STM images were recorded from the same area before and after exposure to water, it can be seen that some of the new OH_b reside in positions previously taken by O_b-vacs. Thus Bikondoa *et al.*[28,65] imaged water dissociating in the O_b-vacs forming one OH_b in place of the O_b-vacs and another OH_b group elsewhere, in line with the mechanism depicted in Fig. 7. Low temperature STM experiments indicate that water dissociation occurs as low as ~187 K,[68] which matches conclusions from high resolution EELS (HREELS).[34]

One curiosity is that the number of OH_b in positions previously taken by O_b-vacs is always slightly higher than the number found elsewhere. According to the mechanism in Fig. 7, an equal number of OH_b should be found at the O_b-vacs and away from them. Wendt *et al.*[67,68] propose that immediately after water molecules dissociate, the two resulting OH_b sit next to each other in the [001] direction. In such a configuration, individual OH_b from the pair are difficult to resolve in STM images and each OH_b pair therefore appears as

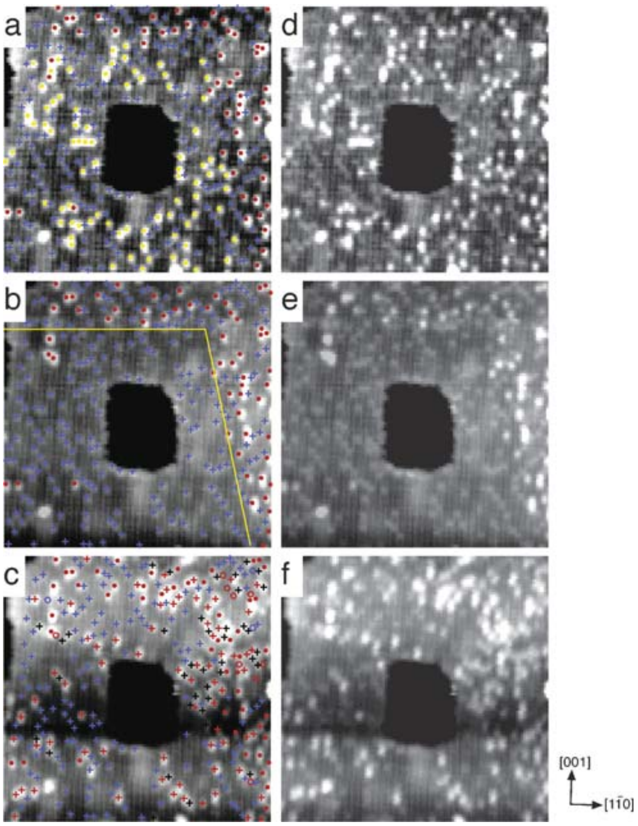

Fig. 11 Sequential (285 Å × 250 Å) STM images of $TiO_2(110)$. (a) As-prepared $TiO_2(110)$ with ∼3.5% and ∼5.5% A_b and A_d defects, respectively. The blue crosses denote A_d defects which are also present in (b), the red circles denote A_b defects, and the yellow circles denote A_b defects which are removed to form the image in (b). (b) Following a +3 V scan. The yellow lines indicate the approximate boundaries beneath which the +3 V scan was applied. Blue crosses and red circles denote A_d and A_b defects, respectively. (c) Following exposure to 0.1 L water. Blue crosses and filled red circles respectively denote A_d and A_b defects which were present in (b). Open red circles indicate positions where A_b defects were present in (b) but not in (c). Red crosses denote new A_b species which reside where A_d defects were positioned in (b) and black crosses denote new A_b species appearing elsewhere. The images are duplicated for clarity in (d), (e), and (f). Modified from ref. 28 with permission.

a single feature, explaining the apparent anomaly. In some images, type-A defects with three apparent sizes can be seen, the largest assigned to OH_b pairs, the next largest to isolated OH_b, and the smallest to O_b-vacs.[65–69] These general trends have been reproduced in the latest STM simulations of O_b-vacs and OH_b.[66,72]

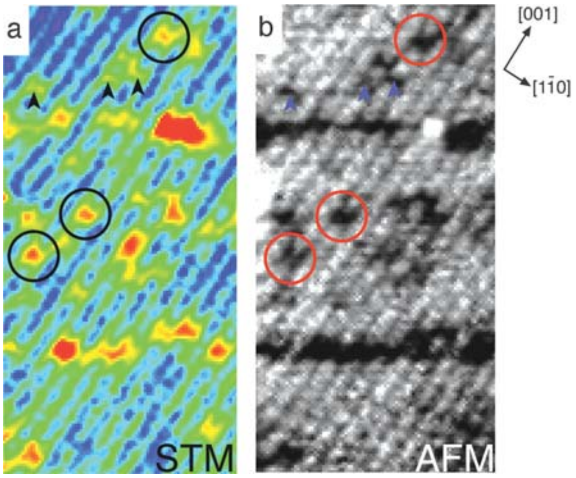

Fig. 12 Simultaneously recorded 80 Å × 150 Å STM and NC-AFM images of $TiO_2(110)$. (a) A colour contoured current map represents the STM image. Because the tip is oscillating during NC-AFM measurements, the *time-averaged* current is recorded.[74] OH_b appear as broad, red spots whereas O_b-vacs appear as narrow, yellow spots. Arrowheads point at three O_b-vacs and circles are drawn over three OH_b, respectively. (b) The simultaneously recorded NC-AFM image. The arrowheads superimposed in blue and the circles superimposed in red both indicate dark depressions. Taken from ref. 73.

The unambiguous assignment of OH_b and O_b-vacs in STM images enabled point defects in NC-AFM images of $TiO_2(110)$ to be identified definitively as well. Fig. 12 shows an STM image alongside a simultaneously recorded NC-AFM image. The STM image was recorded simply by applying a bias between the NC-AFM tip and sample, during otherwise standard NC-AFM operation, and recording the tunnelling current. By correlating the positions of the dark spots in the NC-AFM image with OH_b and O_b-vacs in the STM image, Pang *et al.*[73] show that the dark spots correspond to both OH_b *and* O_b-vacs. It then follows that the bright rows in the NC-AFM image must correspond to O_b rows. The assignment of both OH_b and O_b-vacs (which are in reality protrusions and depressions, respectively) to depressions in the NC-AFM image is significant because it means the intuitive idea that NC-AFM faithfully traces the true surface topography must be rejected.

In further support of this, NC-AFM images recorded by both Pang *et al.*[74] and Lauritsen *et al.*[75] show that adventitious tip changes can give images with differing contrasts. As shown in Fig. 13, Pang *et al.*[74] recorded a pair of NC-AFM images between which such a tip change occurs. In the first image, type-A defects appear as depressions in the bright O_b rows like in Fig. 12b, whereas in the second image, the type-A defects appear as bright features between bright rows; the latter must therefore be assigned to Ti_{5c} rows. One way in which a tip may change is in the polarity of the apex and the observed contrast

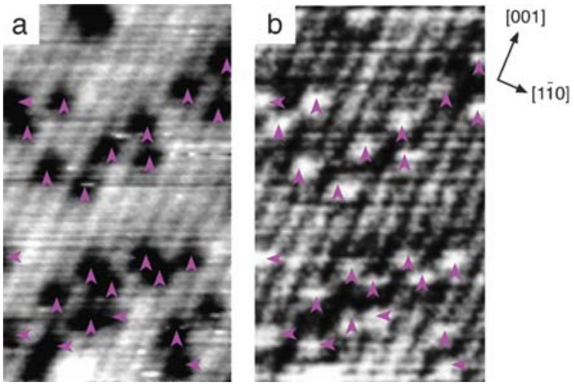

Fig. 13 115 Å × 185 Å NC-AFM images of $TiO_2(110)$. (a) Before the tip change. (b) After the tip change. Purple arrowheads indicate coincident type-A defects. Modified from ref. 74 with permission.

reversal was indeed reproduced in NC-AFM simulations that employed first a tip apex with a positive potential then a negative one.[75]

3.2 Diffusion of water dissociation products

Wendt *et al.*[68] and Zhang *et al.*[69] tracked the diffusion of the OH_b following water dissociation. STM movies at ~187 K showed that the OH_b pairs separate along the $[1\bar{1}0]$ direction *via* proton exchange with water molecules.[68] Snapshots of the movie are displayed in Fig. 14. These movies were supported by calculations of the potential energy profile, which show that the barrier to diffusion is lowered by this exchange with water. Sequential NC-AFM images also capture the splitting of the OH_b pairs at room temperature.[76] The same diffusion mechanism occurs for isolated OH_b and it should be noted that because of the erroneous assignment of OH_b and O_b-vacs by Schaub *et al.*,[64] this water-mediated diffusion of OH_b was mistakenly reported as *oxygen*-mediated diffusion of O_b-vacs,[77,78] *via* a mechanism inconsistent with subsequent isotope studies.[79]

In addition to this water-assisted diffusion, Zhang *et al.*[69] observed OH_b pairs separating along the [001] direction, as shown in Fig. 15. By carefully analysing the positions of the OH_b, it was shown that the first hop is usually taken by the OH_b which does not fill the O_b-vac. Therefore, contrary to previous expectations, the two OH_b resulting from dissociation of a water molecule appear to be inequivalent. Zhang *et al.* speculate that this is due to a different charge distribution around each OH_b; the O_b-vac has two nominally Ti^{3+} ions beneath it so that when water dissociates, the OH_b which sits in the vacancy is connected to two Ti^{3+} ions whereas the adjacent OH_b is bound to only one Ti^{3+} ion, the other Ti ion being Ti^{4+}. It is important to note this description of the charge distribution serves only as an indication that the charge around each OH_b is likely to be different as it is clear from scanned angle PhD that the charge distribution around O_b-vacs is rather complicated (see section 2),[37] and one would expect a similar situation for OH_b.

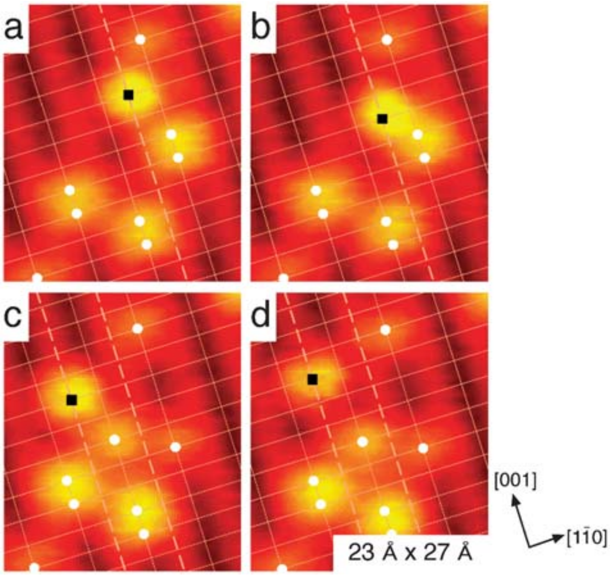

Fig. 14 Sequential images of $TiO_2(110)$ showing the splitting of an OH_b pair mediated by a water molecule at 187 K. OH_b groups are labelled with white circles and water on Ti_{5c} sites is labelled with black squares. Solid grid lines intersect the O_b sites whereas dashed grid lines are along Ti_{5c} rows. Modified from ref. 68 with permission.

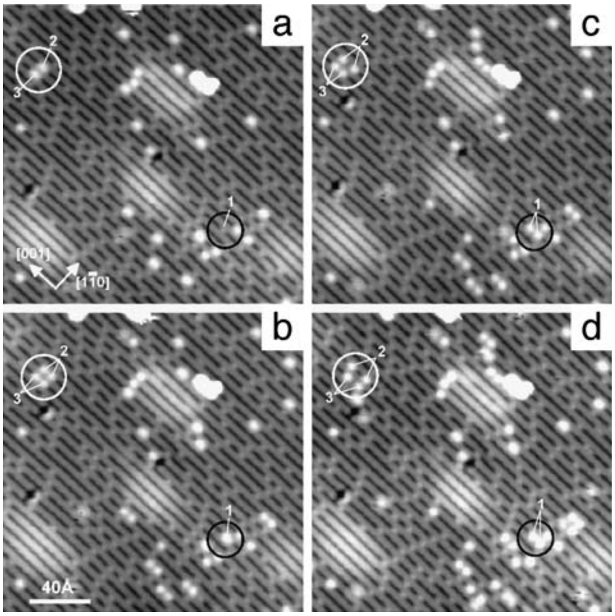

Fig. 15 Sequential STM images recorded as a function of time on water-exposed $TiO_2(110)$. (a) The first image, defined as 0 min, (b) after 21 min, (c) after 35 min, (d) after 50 min. An O_b-vac is labelled '1' in (a) and two OH_b pairs are labelled '2' and '3'. In (b), a water molecule has dissociated to form an OH_b pair in the O_b-vac labelled '1'. The OH_b pairs labelled '2' and '3' in (a) have split into isolated OH_b in (b), separating further in (c) and (d). The new OH_b pair labelled '1' in (b) has separated into isolated OH_b species in (c) and (d). Modified from ref. 69 with permission.

3.3 Water layers

Returning to the water TPD in Fig. 8, measurements by Hugenschmidt *et al.*[57] show that the work function decreases with the coverage of the ~265 K peak. This can be explained by the dipole created if water is molecularly adsorbed with its O atom (O_{water}) pointing down (negative) and the hydrogen up (positive). In such a configuration, one would expect water to sit on the Ti_{5c} sites. This expectation was confirmed in subsequently obtained low temperature STM images.[62,64,67,68] Very recently, this bonding configuration was quantitatively examined with scanned energy mode PhD.[80,81] A Ti_{5c}–O_{water} bond length of 2.21 Å was found, indicating a more weakly bound chemisorbed species in comparison to other adsorbates on $TiO_2(110)$, such as formate (2.08 Å). Given that most theoretical calculations overestimate the Ti_{5c}–O_{water} bond length (*e.g.* refs. 66, 82 and 83), it was suggested that a more accurate theoretical description of this bond could be used as a benchmark in future theoretical modelling.

After the Ti_{5c} sites are filled, a second layer of water can adsorb over the O_b sites corresponding to water in the ~175 K TPD state. Exposures beyond the second layer leads to formation of multilayer water which desorbs at ~163 K in TPD with the zero order desorption kinetics expected.

The work function measurements by Hugenschmidt *et al.*[57] show that water exposure beyond the first monolayer does not lead to any further work function changes. This was taken as evidence that the second layer water adsorbs parallel to the surface, presumably to allow hydrogen bonding to the first layer water. An O–H stretch appeared in HREEL spectra below ~3300 cm^{-1} when the second layer of water was adsorbed. As stretching frequencies below ~3400 cm^{-1} are typical of hydrogen bonded OH,[84] the feature below ~3300 cm^{-1} suggests that the second layer water is hydrogen bonded. However, as the loss feature assigned to the monolayer remained at ~3505 cm^{-1}, neither shifting nor attenuating, Henderson[58] concluded that the hydrogen bonding does not involve the O–H bonds of monolayer water.

New evidence has recently been given for hydrogen bonding between monolayer and second layer water molecules by an ESD study. Crucially, Petrik and Kimmel were able to form isotopically distinct bilayers of water.[85] A monolayer of water was prepared by dosing one water isotope at 195 K. The second layer could then be prepared by dosing another water isotope below 70 K. By monitoring water evolution during ESD at temperatures above 70 K, Petrik and Kimmel gave evidence for H–D exchange above 70 K and interlayer mixing of molecules above 90 K. Thus, it was concluded that the second water layer hydrogen bonds to the monolayer. When thicker water films (~3 ML) were electron bombarded at ~100 K,[86] H and H_2 were detected, indicating that the bombardment causes water to dissociate.

3.4 Water at ambient pressures

Ketteler *et al.*[87,88] used a specially designed ambient pressure PES system to investigate water adsorption on $TiO_2(110)$ under pressures of up to ~2 mbar. This was performed by tracking the respective core level PES signals from oxygen originating from molecular water and OH_b. At the beginning of the measurements, the OH_b coverage was twice the initial O_b-vac coverage, indicating that water had dissociated in the O_b-vacs, as expected on the basis of UHV experiments (see section 3.1 and refs. 28, 65–69). As the water coverage was increased, either by decreasing the temperature at a fixed pressure (isobars) or by increasing the pressure at a fixed temperature (isotherms), the OH_b concentration remains the same, showing that no further water dissociation occurred beyond that already attributed to O_b-vac dissociation.

The isotherms and isobars can be converted into a relative humidity measurement (RH) which is defined as $p/p_v(T) \times 100$, where p is the pressure and p_v is the equilibrium vapour pressure of bulk water or ice at the corresponding temperature (T). When the isobars and isotherms are plotted together, they follow the same curve. This indicates that the vapour and surface are in thermodynamic equilibrium. Fig. 16 shows coverage *versus* RH curves for three isobars. The water coverage increases steadily with RH then plateaus as the OH_b coverage is approached, after which the water coverage increases again with inflections at ~2 ML and ~3 ML.

From these results, Ketteler *et al.* suggest that OH_b act as Brønsted acid sites, binding water into OH_b–H_2O complexes. These complexes themselves nucleate further water adsorption. As more water attaches to these nucleation centres, the adsorption complex becomes less acidic and the water binding structure tends to that of the bulk liquid. This is achieved after adsorbing ~2 ML of water.

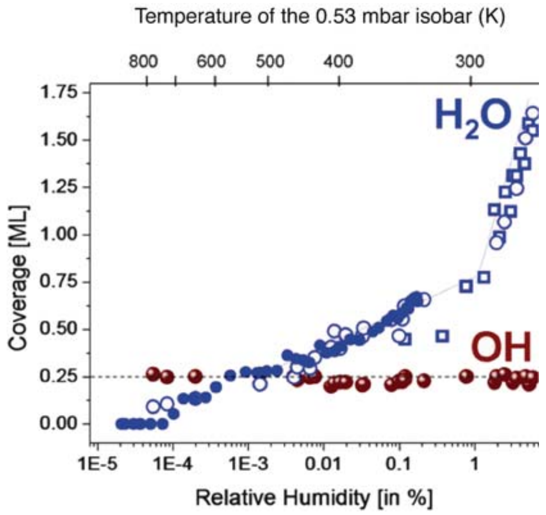

Fig. 16 Coverage of OH_b and H_2O obtained from three different isobars (1.33×10^{-2} to 2 mbar) as a function of relative humidity (RH). Filled blue circles are from the ~0.01 mbar isobar, open circles the ~0.53 mbar isobar, and open squares from the ~1.33 mbar isobar. The temperature scale at the top corresponds to the 0.53 mbar isobar. There is a plateau for water at 0.25 ML when the coverage equals that of OH_b. Modified from ref. 88 with permission.

4. Oxygen

O_2 like water is often present in environments where TiO_2 might be used in technological applications. Added to this, the interaction of O_2 and TiO_2 is of direct importance in devices such as solar cells, gas sensors, and catalytic converters. In this section, we focus first on O_2 adsorption chemistry. In particular, we consider examples of dissociative and molecular adsorption as well as co-adsorption with water, before discussing the reoxidation of the surface at high temperature.

4.1 O_2 dissociation

Numerous studies show that when $TiO_2(110)$ is exposed to O_2, the O_b-vacs are healed. Kurtz *et al.*[33] used resonant PES to show that when O_2 is dosed at 400 K the BGS associated with O_b-vacs is essentially quenched with O_2 exposure. Similar results were obtained by Pan *et al.*[89] and Wang *et al.*[35], the latter employing defective surfaces prepared by electron bombardment.

Onda *et al.*[36] used 2PP spectroscopy to compare O_2 adsorption on defective surfaces created by electron bombardment and vacuum annealing. Their results suggest that defects created by electron bombardment perturb the work function less than those created by vacuum annealing. Furthermore, Onda *et al.* found that the BGS introduced by electron bombardment was quenched by only 0.3 L O_2 at 100 K. In contrast, for a defective surface created by UHV annealing, Perkins and Henderson[90] reported that the BGS detected by EELS was only removed after annealing the surface to 200 K, following exposure to O_2 at 110 K. Onda *et al.*[36] conclude that electron bombardment can lead to pure O_b-vac creation whereas vacuum annealing probably generates a variety of defects, only some of which are O_b-vacs.

Pan *et al.*[89] prepared an oxidised surface by annealing and cooling $TiO_2(110)$ in 2.7×10^{-6} mbar O_2. Low energy ion scattering (LEIS) from this surface showed no ^{18}O uptake even after exposure to 500 L $^{18}O_2$ at room temperature. On the other hand, when an equivalent experiment was performed on a UHV annealed surface, the ^{18}O uptake had a saturation value of ~0.08 ML, consistent with estimates of the O_b-vac density.[33]

Whilst these results indicate that exposure to O_2 heals the O_b-vacs even at low temperatures (at least based on the electronic structure), the healing mechanism is yet to be addressed. Epling *et al.*[91] posited four feasible scenarios whereby O_b-vac may be healed by O_2: (1) two O_b-vacs are filled by one O_2 molecule, (2) one O_b-vac is filled by an O atom from one O_2 molecule with the other O atom being released into the gas phase, (3) one O_b-vac is filled by an O atom from one O_2 molecule with the other O atom being incorporated into the bulk, and finally (4) one O_b-vac is filled by an O atom from one O_2 molecule with the other O atom being adsorbed at the surface, most likely at a Ti_{5c} site.

Epling *et al.*[91] show that adsorbed oxygen in some form is left on the surface after the O_b-vacs are filled. The evidence comes from the perturbation of the TPD spectra of water and ammonia when the surface is pre-dosed with O_2. For a $TiO_2(110)$ surface pre-dosed with O_2 at 300 K, then exposed to water at 90 K, a new water TPD peak is found at ~290 K. Scenarios (1)–(3) above should not have any effect on the reactivity of the $TiO_2(110)$ surface, so it was concluded that one O_b-vac is healed per O_2 molecule with the other O atom being adsorbed at a Ti_{5c} site (O_{ad}), a dissociation mechanism supported by theoretical calculations.[92,93]

The ~290 K peak can be explained as follows: water reacts with the O_{ad} to form two OH groups bound to the Ti_{5c} sites (OH_t groups). As the temperature is ramped towards 300 K, water is desorbed, leaving an O_{ad} at the surface again. To test that O_{ad} is still present following desorption of water in the ~290 K peak, Epling *et al.*[91] first dosed O_2 then water at 90 K. A water TPD spectrum was then taken to 550 K with the new peak at ~290 K again appearing. Cooling the sample to 90 K and re-dosing water *without* further O_2 exposure led to an almost identical spectrum. Isotopic studies show that the water which desorbs at ~290 K scrambles oxygen from O_{ad} and oxygen from the dosed water, consistent with the proposed mechanism.

An indication of the temperature range at which O_{ad} is formed by O_2 dissociation can be obtained by varying the O_2 exposure temperature and measuring the area under the ~290 K peak in otherwise identical TPD spectra. The peak area decreased slightly between 300–375 K and significantly between 530–650 K. The sharp decrease above 530 K can be attributed to competition between dissociation of O_2 to form O_{ad} and the reoxidation of the surface where oxygen is incorporated into the growing $TiO_2(110)$ crystal, a process which will be discussed further in section 4.4. Although there was no change in the ~290 K peak area for O_2 exposed at 90 K and 300 K, this does not necessarily mean O_2 dissociates at the lower temperature because O_2 molecules could adsorb molecularly at the lower temperature, then dissociate as the temperature is ramped towards ~290 K.

Bikondoa *et al.*[28,65] imaged the dissociation of O_2 directly using STM. They ensured that any O_2 reaction with O_b-vacs was not convoluted with O_2/OH_b reactions by removing OH_b from an area of the surface by scanning at +3 V. The same area was then imaged before and after exposure to ~0.6 L O_2 at room temperature, as shown in Fig. 17. Following O_2 exposure, the four O_b-vacs indicated in Fig. 17a are replaced with four bright features on nearby bright rows. This indicates that O_2 has dissociated in the O_b-vacs, with one O atom filling the vacancy and the other forming O_{ad} on a nearby Ti_{5c} site. Wendt *et al.*[67] obtained similar results with O_2 dosed at 120 K, showing that O_2 dissociates in O_b-vacs at least down to 120 K.

Spatial analysis of the O_{ad} positions following dissociation at room temperature reveal ~74% of them lie one lattice constant (in the [001] direction) away from the O_b-vac filled, the other ~26% being found immediately adjacent and two

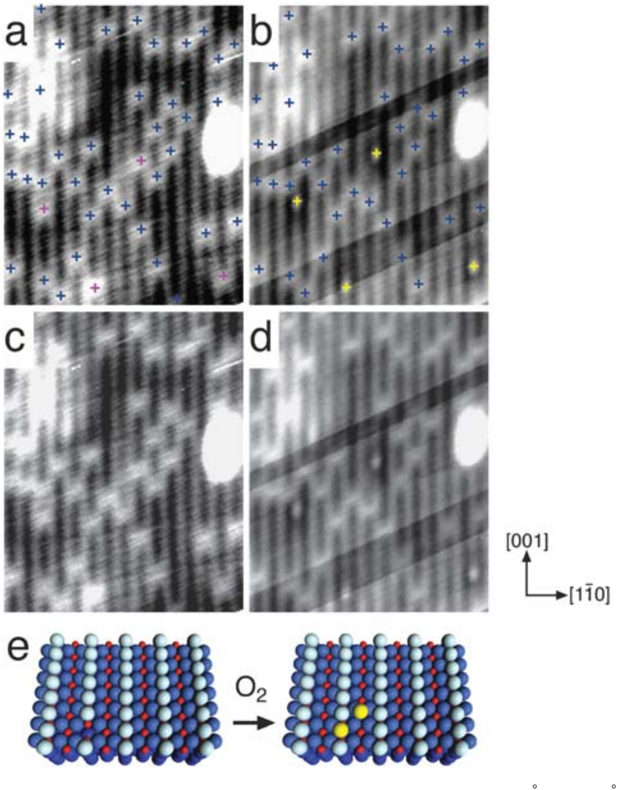

Fig. 17 Reaction of O_2 with O_b-vacs on $TiO_2(110)$. (a) 100 Å × 120 Å STM image of $TiO_2(110)$ following a +3 V scan to remove OH_b. The O_b-vacs are marked with blue crosses except for four O_b-vacs that do not appear in (b) which are instead marked with purple crosses. (b) STM image with the same size and scan parameters as (a), following exposure to 0.6 L O_2. O_b-vacs which coincide with those in (a) are indicated with blue crosses. Bright spots which appear on the bright rows, near to the position of the O_b-vacs in (a), are indicated with yellow crosses. The images are duplicated for clarity in (c) and (d). (e) Schematic representation of the reaction. Oxygen originating from the exposed O_2 is coloured yellow. The O_{ad} is positioned diagonally adjacent to the O_b-vac after Du *et al.*[94] Modified from ref. 28 with permission.

lattice constants away.[94] As thermal diffusion of O_{ad} on $TiO_2(110)$ is very slow, the separation of O_{ad} from the positions adjacent to the reacting O_b-vacs was attributed to energy released during the exothermic dissociation of the O_2 molecule (calculated at $\sim$3.5 eV[67]) in a similar way to that observed for Cl_2 dissociation.[95]

4.2 Molecular adsorption of O_2

A surprising temperature dependence was observed for $TiO_2(110)$ surfaces exposed to O_2. At 120 K, Henderson *et al.*[96] reported that up to three O_2 molecules were adsorbed per O_b-vac. As these surfaces are heated, one O_2 per O_b-vac dissociates. The other O_2 molecules desorb molecularly at $\sim$410 K. As the adsorption temperature is increased, the amount of O_2 desorbed in the $\sim$410 K state is reduced until the state disappears at an adsorption temperature of 180 K. It was therefore concluded that at $\geq$ 180 K, no molecular O_2 adsorbs. After TPD to 435 K, re-exposing the surface to O_2 at 120 K does not revive the $\sim$410 K O_2 peak in TPD. Henderson *et al.*[96] conclude that whilst the additional molecularly adsorbed O_2 may not adsorb directly in the O_b-vac, they adsorb in sites somehow associated with them, such as in adjacent sites.

Alongside this rich thermal chemistry, a series of photoreaction and photodesorption experiments have been performed.[90,97–101] Lu *et al.*[97] found two molecular chemisorption states for O_2 which were denoted as α and β states. Upon UV irradiation, the α state photo-oxidises CO whereas the β state undergoes fast photodesorption. When O_2 is adsorbed at a temperature of $\sim$105 K, the α state dominates. Annealing above $\sim$200 K converts the α state to the β state. Above $\sim$300 K, the α state is no longer present and the β state disappears above $\sim$400 K. As with the thermal experiments, these molecular O_2 states were linked to O_b-vacs. This was based on their maximum saturation density (0.12 ML) which compared well with typical estimates of the O_b-vac density.[89]

Further experiments led to the α state being resolved into two states (α_1 and α_2) with different photodesorption cross-sections.[98] However, very recently, Thompson and Yates have proposed that rather than the existence of multiple O_2 species, the desorption rate of O_2 follows a fractal rate law,[102] whereby the rate 'constant' varies with the time of the reaction and is therefore more correctly described as a rate *coefficient*.[99,101]

By irradiating a $TiO_2(110)$ surface exposed to O_2 at $\sim$115 K with UV light prior to performing TPD measurements, Perkins and Henderson showed that the $\sim$410 K O_2 TPD peak depletes.[90] Because the α_2 state was reported to dominate at such a low temperature and because the cross-section for depletion of the $\sim$410 K TPD peak is close to that reported for photodesorption of the α_2 state, Perkins and Henderson assigned the $\sim$410 K state to α_2 O_2. However, Thompson and Yates disagree with this assignment, based on the observation that the α states already convert to the β states at 300 K, which themselves dissociate by $\sim$400 K.[100] Hence, the connection between these thermally and optically activated O_2 molecules is still open to debate. Nevertheless, both sets of experiments point to molecular adsorption of O_2 at low temperatures provided that O_b-vacs are present. However, in contrast to this, Wendt *et al.* suggest that some minority sites apart from O_b-vacs must be responsible for the molecular adsorption of O_2 because they find that even at 120 K, O_2 dissociates to form O_{ad}.[67]

4.3 O_2 and water reactions

In section 4.1, we described how water reacts with a $TiO_2(110)$ surface pre-exposed to O_2. Here, the order of adsorption is reversed and the effect of dosing O_2 on a surface pre-exposed to water is examined.[34] Water TPD spectra recorded from a hydroxylated $TiO_2(110)$ surface exposed to O_2 gives rise to a new peak at $\sim$300–320 K which intensifies at the expense of the $\sim$520 K peak when the O_2 exposure is increased. The $\sim$520 K peak corresponds to the OH_b recombinative peak at $\sim$490 K in section 3.1, the recorded temperatures of the TPD peaks being systematically offset from the earlier work. Similarly, the $\sim$300–320 K peak corresponds to the $\sim$290 K OH_t recombinative peak found when a $TiO_2(110)$ surface with O_{ad} is exposed to water (section 4.1).

By isotopically labelling the O_2, it was shown that the water which desorbs at $\sim$300–320 K always comes from the dosed O_2 and not from lattice O. This means that O_2 must abstract hydrogen from OH_b presumably to form OH_t. H_2O_2 and/or O_2H were speculatively suggested as intermediate species before conversion to OH_t, with subsequent calculations showing that H_2O_2 is particularly stable.[103]

4.4 Reoxidation of non-stoichiometric $TiO_2(110)$

As far back at the 1960s, it has been known that TiO_2 surfaces are reduced during ion sputtering and that the stoichiometry is restored during annealing, even in UHV. There had been an assumption in the literature that this stoichiometry is restored by diffusion of oxygen from the bulk to the surface. However, in the past decade or so, there has been a growing body of work which supports the idea that stoichiometry is also restored by the diffusion of reduced Ti^{n+} interstitial ions back into the bulk.[104,105] By annealing $TiO_2(110)$ samples in pressures of O_2, the reoxidation of these interstitial ions has been stunningly captured in a series of high temperature STM and low energy electron microscopy (LEEM) experiments.

Onishi and Iwasawa were the first to image this reoxidation process directly. They recorded STM images of the $TiO_2(110)$ surface reacting with O_2 (1×10^{-7} mbar) over a period of about 40 min. 1×2 rows were observed growing out from 1×1 terraces, leading to the conclusion that interstitial Ti^{n+} ions react with O_2 at the surface to form added Ti_2O_3 rows.[41]

This reoxidation process has been studied in more detail with a series of high resolution STM movies by Bowker *et al.*[51,106–108] and Bennett.[109] The movies can be viewed *via* refs. 106 and 109. Both the simple 1×2 and x-linked 1×2 rows were observed to reoxidise, although the x-linked 1×2 was found to be more reactive to oxygen.[51]

Fig. 18 shows a sequence of STM images recorded at 673 K and $\sim 4 \times 10^{-7}$ mbar O_2, starting with an image of x-linked 1×2. As the reaction progresses, the density of x-links increases until they fill in the gaps between the 1×2 rows and small 1×1 patches are formed (Fig. 18c). Continued reaction with O_2 leads to the coalescence of the 1×1 patches until

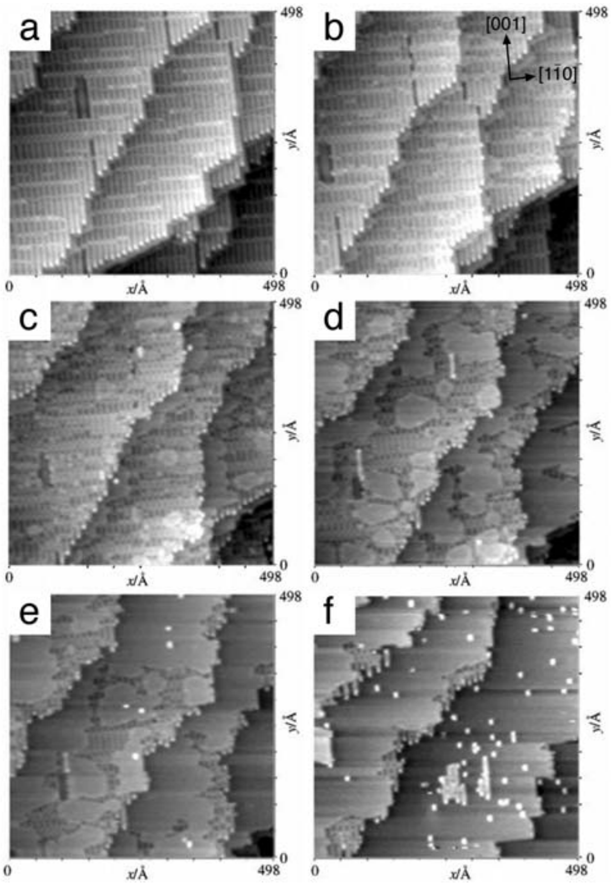

Fig. 18 Reoxidation of the x-linked 1×2 surface at 673 K in the presence of ∼4 × 10^{-7} mbar O_2. Modified from ref. 107 with permission.

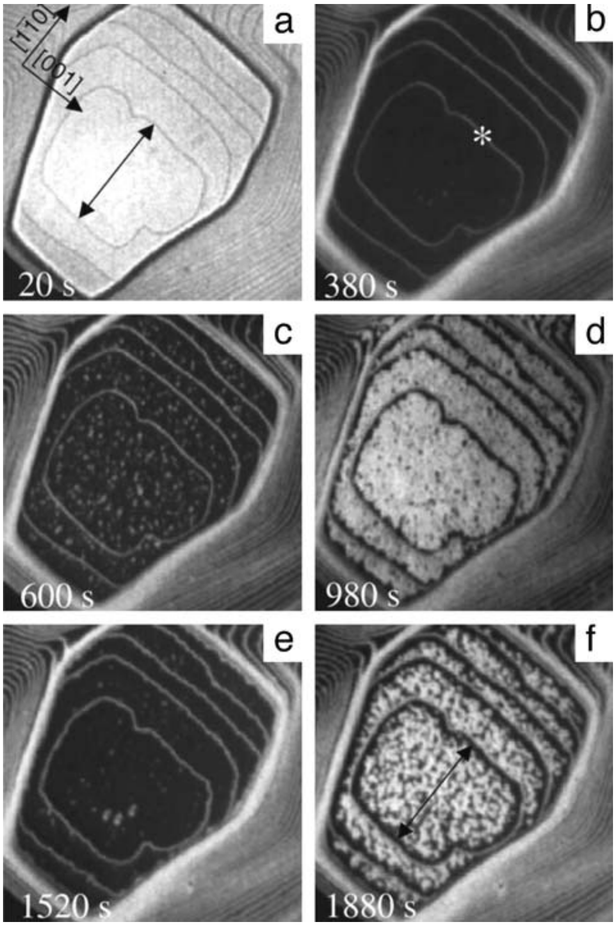

Fig. 19 Sequential (2.6 μm)^2 LEEM images as a medium-blue $TiO_2(110)$ crystal is exposed to 1.3 × 10^{-6} mbar O_2 at 820 K. Before oxygen exposure, which began at 0 s, the crystal had 1×1 structure. The intensity of the bright-field images oscillates during exposure. Double-ended arrows drawn on (a) and (f) show that the initial terraces do not move. Modified from ref. 110 with permission.

almost none of the original 1×2 terrace remains (Fig. 18e), whereupon 1×2 rows grow on top of the 1×1 surface and the 1×2 → 1×1 → 1×2 cycle continues.

The same cyclic growth can be seen on a much larger scale in the series of LEEM images shown in Fig. 19, which were recorded at 820 K and 1.3 × 10^{-6} mbar O_2.[110] The images in Fig. 19 are set so that the dark areas correspond to the 1×2 phase and the bright areas the 1×1 phase. At the start of the experiment, the surface has a 1×1 termination (Fig. 19a). The surface has switched to a 1×2 phase in Fig. 19b. In Fig. 19c, 1×1 areas have nucleated on the 1×2 surface, almost filling the surface in Fig. 19d, whereupon the 1×1 → 1×2 → 1×1 → 1×2 cycle continues.

While both the STM and LEEM sequences show the basic reoxidation reaction, exploration of the parameter space reveals subtle differences in the reaction depending on the temperature and pressure. Most notably, both the STM and LEEM experiments reveal a competition between growth out of the surface (layer-by-layer) and growth of the surface laterally (step-flow) with step-flow dominating at higher temperatures. Step-flow is shown clearly in Fig. 20. At intermediate temperatures, a mixed growth mode occurs whereby the larger terraces grow in the layer-by-layer fashion and the smaller terraces grow by step-flow until they reach a critical size. At the critical size, layer-by-layer growth begins.[110] At low temperatures (<573 K at 1 × 10^{-7} mbar O_2 in ref. 106) and high temperatures (>1023 K in 1.3 × 10^{-6} mbar O_2 in ref. 110) little or no reactivity was observed. For low temperatures, this is presumably because the thermal energy supplied

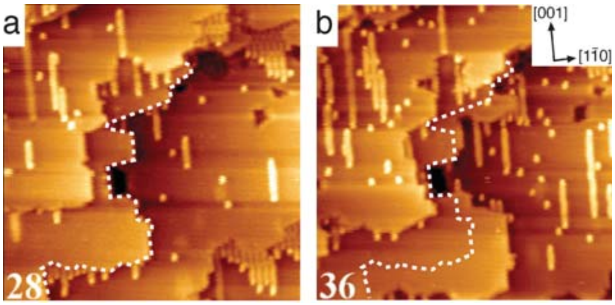

Fig. 20 Two (500 Å)^2 frames from movie 3 of ref. 106 recorded at 773 K in ∼1 × 10^{-7} mbar O_2. The STM image in (a) was taken 400 s before that in (b). A dotted white line traces the edge of a 1×1 step edge. The white line is superimposed on the image in (b) showing clearly that the step edge has grown away from the previous boundary. The frames are reproduced with permission.

is insufficient to overcome the barriers to reaction, whereas at high temperatures the surface growth is limited by the low residency time of the O_2 molecules at the surface. With the data available, it is not yet possible to form a useful 'phase diagram' for the growth modes. Whilst McCarty varied the O_2 pressure around 1.3×10^{-6} mbar to establish qualitatively that the transition temperature between layer-by-layer/mixed/pure step-flow increases with O_2 pressure, this has not been recorded quantitatively. More difficult will be accounting for the Ti interstitial concentration between different crystals. So far, this has largely been done simply by noting the colour of the crystal. One way in which the Ti interstitial density could be quantified is by measuring the resistivity of the crystal.[38]

Li *et al.*[38,111–113] performed a series of studies somewhat different to the previous ones in that the samples are reoxidised in O_2 ($\sim 1 \times 10^{-6}$ mbar), then imaged at room temperature without O_2 present. A new surface morphology was found consisting of a pseudo-hexagonal network. The structure was assigned to an incomplete 1×1 layer which forms on top of the 'normal' 1×1 termination. It was termed a 'rosette' network and forms at ∼470–660 K. The rosettes are reminiscent of the 1×2 x-links and it is likely that at least parts of a spongy surface formed by Stone *et al.*[106] at ∼573 K have the same structure.

Importantly, Li *et al.*[112] have also reoxidised their crystals with $^{18}O_2$ and detected ^{18}O incorporation at the surfaces, finding a maximum rate for ^{18}O incorporation at ∼669 K. Li *et al.* also found ^{18}O uptake to be faster for more reduced crystals (as judged qualitatively from their colour).[112] This indicates that the growth rate is dependent on the concentration of Ti^{n+} interstitials. A similar reaction dependence was also observed by McCarty,[110] and was one of the reasons suggested for the different activation energies for reoxidation calculated by Smith *et al.*[108] (∼25 kJ mol^{-1}) from extended sequences of STM images and by Li *et al.*[112] (∼80 kJ mol^{-1}) from ^{18}O uptake measurements.

5. Carboxylic acids

Given the importance of carboxyl containing molecules in a variety of TiO_2-based applications (*e.g.* Grätzel-type solar cells), it is hardly surprising that there is a large archive of fundamental studies on the interaction of carboxylic acids with $TiO_2(110)$. Effort has largely focused on adsorption on the 1×1 phase, although there are also studies of the chemistry on the 1×2 reconstruction.

In this section, the chemistry of the simplest carboxylic acid, namely formic acid, is first discussed, covering both initial adsorption and subsequent decomposition. Then we move onto other carboxylic acids, discussing their adsorption, thermal decomposition, and finally photodecomposition.

5.1 Formic acid

5.1.1 Adsorption. It is well established[114–117] that formic acid adsorbs dissociatively (acidic hydrogen cleavage) on $TiO_2(110)1\times1$ at room temperature, *i.e.*

$$HCOOH_{(g)} \rightarrow [HCOO]^-_{(ads)} + H^+_{(ads)} \qquad (1)$$

These chemisorbed formate species ($[HCOO]^-_{(ads)}$) saturate at approximately 0.5 ML (where 1 ML corresponds to one formate per surface 5-fold Ti), forming an ordered (2×1) overlayer.[114] At lower formate coverage, a local c(4×2) order has been observed with STM.[118]

To gain further insight into the acid dissociation reaction, several groups have probed the geometry of the surface formate moiety.[116,117,119–122] Of these investigations the most detailed is a chemical-state specific scanned-energy mode PhD study by Sayago *et al.*,[122] which quantitatively determines both bonding site and adsorbate orientation. It is concluded that formate binds to the surface through both of its oxygens to two adjacent five-fold surface titanium (Ti_{5c}) atoms, so that its molecular plane is aligned with the [001] azimuth, *i.e.* it lies parallel to the rows of bridging oxygens (O_b). A schematic diagram of this local adsorption geometry is shown in Fig. 21, including values for pertinent structural parameters. Interestingly, the location of the proton ($H^+_{(ads)}$) resulting from HCOOH dissociation was also determined in this study. It was found to be attached to a bridging oxygen, forming a bridging hydroxyl (OH_b).

Other experiments,[116,117,119–121] as well as theoretical calculations,[123–127] support the formate adsorption geometry determined by Sayago *et al.* (Type A in Fig. 22). In addition, some measurements suggest the presence of a second formate species on $TiO_2(110)1\times1$.[116,117,121,128] From reflection absorption infra-red spectroscopy (RAIRS)[116] and near edge X-ray absorption fine structure (NEXAFS),[121] it was concluded that this second formate comprises ∼30–40% of a saturated (2×1) overlayer, and is oriented with its molecular plane aligned along the $[1\bar{1}0]$ direction, *i.e.* it is azimuthally rotated by 90° with respect to Sayago *et al.*'s formate configuration. It was suggested in ref. 116 that this species is Type B in Fig. 22, which arises through reaction of formic acid with O_b-vacs, generated during the formation of Type A formate. This Type B configuration, which is coordinated *via* one O to the O_b-vac and through its other O atom to an adjacent Ti_{5c} site, was first proposed by Wang *et al.* on the basis of *ab initio* calculations.[123]

Sayago *et al.* found no evidence for the second formate species, although they did consider such a possibility during their structure determination.[122] Long-range order is not a prerequisite for application of PhD, and so a minority formate species, if present in sufficient concentration, would emerge

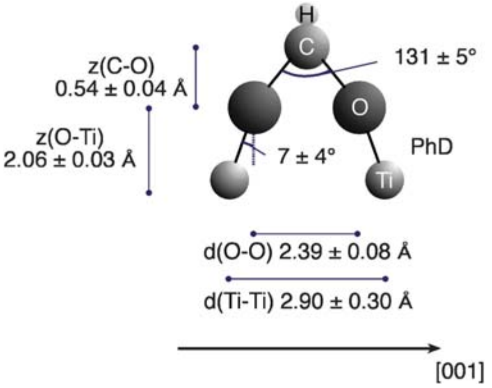

Fig. 21 Schematic diagram of the local formate adsorption geometry, indicating various best-fit structural parameters derived from PhD.[122]

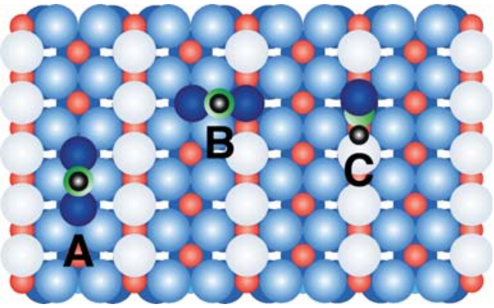

Fig. 22 Schematic plan view of $TiO_2(110)1\times1$, illustrating three formate adsorption geometries, namely Type A, Type B, and Type C.

from the data analysis. Consequently, there appears to be a significant disparity between the PhD, and the RAIRS and NEXAFS studies.[116,121] However, as indicated in ref. 122, it may merely be that the population of Type B formate is minimal in the PhD study due to differences in experimental conditions, *e.g.* sample preparation/history, amount of formic acid dosed, and the precise substrate temperature during exposure. Recent work by Aizawa *et al.*[129] supports this hypothesis. They acquired STM images from a $TiO_2(110)1\times1$ surface exposed to formic acid and then annealed to 350 K for 400 min. Careful analysis of the data indicated three different formate surface geometries, Type A, Type B, and Type C in Fig. 22, which were present on the surface in a ratio of 10 : 7 : 3. Type C formate is surface bonded through only one O atom, which fills an O_b-vac. Given these results, it is plausible that the second formate species observed in RAIRS and NEXAFS is a result of formic acid exposure being conducted with the substrate somewhat above room temperature. We note that STM images recorded by Bowker *et al.*[128] following formic acid dosing at room temperature are also suggestive of a second formate species, but at a concentration of only ~1% of the ordered (2×1)-$[HCOO]^-$ overlayer.

In contrast to this extensive effort on the 1×1 phase, there has been very limited activity focusing on the adsorption of formic acid on reconstructed $TiO_2(110)$. Bennett *et al.*[130] have employed STM to examine formic acid adsorption at room temperature on the x-linked 1×2 phase. They found that formic acid binds, presumably as formate, preferentially to the x-links, although it does also adsorb in between the x-links, forming a rather disordered overlayer. In another STM study[25] on a $TiO_2(110)$ surface exhibiting strands of the simple 1×2 phase, it was concluded that formic acid does not adsorb on these features. Bennett *et al.* used this result as evidence that the simple and x-linked 1×2 phases have different structures. However, given that more recent work suggests that these two phases both consist of Ti_2O_3 added rows (see section 2), it is more likely that this difference in surface reactivity is due to variation in experimental procedure. For example, Bennett *et al.*[130] exposed the surface to ~240–500 L of formic acid, whereas an exposure of 3 L was employed in ref. 25.

5.1.2 Thermal decomposition.

Aizawa *et al.*'s STM study[129] was motivated by interest in understanding the thermal decomposition of formic acid on $TiO_2(110)1\times1$ beyond surface formate formation. This topic has been a focus of attention for a number of years, and quite detailed insight has been gained through a combination of experiment and theory. The former effort can be separated into two categories, namely measurements performed with the $TiO_2(110)$ sample at fixed temperature in a flux of formic acid (*i.e.* steady-state conditions) and studies of adsorbed formic acid/formate overlayers as a function of substrate temperature.

Under steady-state conditions, Onishi *et al.*[114,131] conclude that there are two decomposition channels for formic acid on $TiO_2(110)1\times1$, *i.e.*

$$HCOOH_{(g)} \rightarrow CO_{(g)} + H_2O_{(g)} \text{ (dehydration)} \qquad (2)$$

and

$$HCOOH_{(g)} \rightarrow CO_{2(g)} + H_{2(g)} \text{ (dehydrogenation)} \qquad (3)$$

They have found that the dehydration reaction is dominant at substrate temperatures >500 K, whereas at lower temperatures dehydration prevails. A similar result emerged from a comparable study by Wang *et al.*[132] In sharp contrast, Bowker *et al.*[128] found no evidence for the dehydrogenation reaction in their steady-state measurements, observing only dehydration. There is no obvious explanation for this discrepancy, although it has been suggested it might be due to differences in either formic acid partial pressure or surface structure.[128,132] We note that Bowker *et al.*[128] did observe formic acid dehydrogenation on a surface decorated with Pd nanoparticles.

As regards the evolution of formic acid/formate overlayers with temperature, it has been found that by approximately 350 K any long-range (2×1) order is lost.[114] This disordering arises due to the formation of multiple formate bonding geometries,[129] as discussed above, along with desorption of a proportion of the bound formate, which TPD shows comes off as formic acid,[114,115,132] *i.e.*

$$[HCOO]^-_{(ads)} + H^+_{(ads)} \rightarrow HCOOH_{(g)} \text{ (recombination)} \qquad (4)$$

Besides evidencing this recombination reaction, desorbed species observed in the TPD measurements also reveal surface formate decomposition processes; a list of the desorbed species and their desorption temperatures (T_Ds) found in the three TPD studies conducted to date[114,115,132] is provided in Table 3. In all of these studies, CO and H_2O are both major products, suggesting that formic acid dehydration (reaction (2)) readily occurs under these conditions. Most simply, this reaction could proceed through fragmentation of the adsorbed formate,

$$[HCOO]^-_{(ads)} \rightarrow CO_{(g)} + OH^-_{(ads)} \qquad (5)$$

with the resulting hydroxyl species combining with the previously dissociated acidic hydrogen (reaction (1)) to form water. Interestingly, however, although some water desorbs at approximately the same temperature as CO ($T_D \sim 560$ K), the majority leaves the $TiO_2(110)$ surface at a significantly lower temperature ($T_D \sim 350$–440 K). On the basis that any CO formed would immediately desorb at these substrate temperatures,[115] the lower temperature water TPD feature must arise from a process unrelated to formate decomposition (reaction (5)). TPD from an ^{18}O-enriched $TiO_2(110)$, in

Table 3 Desorbed species and their desorption temperatures from three separate TPD experiments[114,115,132] performed on $TiO_2(110)1\times1$ exposed to formic acid (HCOOH or DCOOD). Onishi *et al.*[114] acquired their data following formation of a (2×1) formate overlayer at 230 K. Wang *et al.*'s data[132] were recorded after a saturation exposure at room temperature. Except for the values for CO_2, the entries for Henderson's work[115] are for a substrate ($T \sim 100$ K) exposed to sufficient formic acid to form approximately a monolayer; the CO_2 data derive from a surface prepared similarly to that of Wang *et al.* Only desorption above room temperature is recorded

	Desorption temperature/K		
Desorbed species	Onishi *et al.*[114]	Wang *et al.*[132]	Henderson[115]
H_2[115]/D_2[114,132]	400	444	—
	570	575	
H_2O[115]/D_2O[114,132]	350	438	350–400
	570	577	580
C_2H_2	—	—	580
CO	570	567	555
H_2CO[115]/D_2CO[114,132]	—	575	548
CO_2	570	475	380–600
		585	
HCOOH[115]/DCOOD[114,132]	350	411	400
	570	564	538

combination with HREELS and SSIMS,[115] suggest that this water is produced through the following reaction:

$$OH_b{}^-{}_{(ads)} + OH_b{}^-{}_{(ads)} \rightarrow H_2O_{(g)} + \text{O-vac} \qquad (6)$$

where the hydroxyl species are those formed upon dissociative adsorption of formic acid (reaction (1)). Given that these hydroxyl species are bridging hydroxyls,[122] the O-vac in reaction (6) is almost certainly an O_b-vac, as illustrated in Fig. 23. This deduction is supported by Bowker *et al.*'s[128] STM images from a formic acid exposed $TiO_2(110)1\times1$ surface annealed to 420 K, which indicate the presence of significant quantities of O_b-vacs. We note that when water is dosed onto a clean surface (see section 3.1) recombinative desorption (reaction (6)) occurs at ~490 K, so it is not clear why these OH_b species recombine at an apparently lower temperature here (350–440 K).

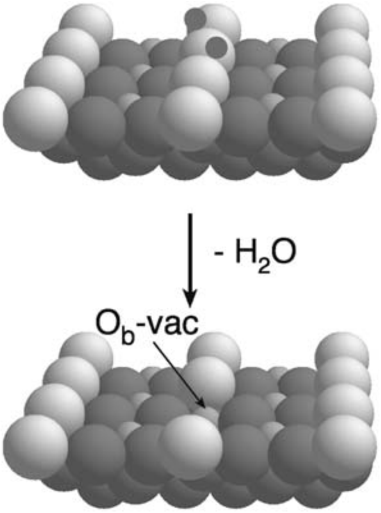

Fig. 23 Schematic depiction of O_b-vac formation through the combination of bridging hydroxyls to form water.

HREELS elastic peak measurements[115] indicate that these O_b-vacs do not persist at higher temperatures, but are healed in coincidence with the onset of formate decomposition. This result suggests that defects of this type are integral to the decomposition chemistry of formic acid on $TiO_2(110)1\times1$, *i.e.* surface formate species interact directly with O_b-vacs during decomposition. Accordingly, Wang *et al.*[132] have proposed that formate decomposition is initiated by the following step,

$$[HCOO]^-{}_{(ads)} + O_b\text{-vac} \rightarrow [HCO]^-{}_{(ads)} + O_b \qquad (7)$$

They suggest that $CO_{(g)}$ is then generated by loss of hydrogen from the surface formyl species ($[HCO]^-$). In addition, this reaction also explains the presence of formaldehyde (H_2CO) in the list of desorbed species in Table 3, as it can easily be formed by combining formyl with a surface hydroxyl hydrogen. (We note that as a consequence of reaction (7) formate oxygen should be incorporated into the $TiO_2(110)$ surface, and that this process has been validated by Henderson.[115])

A more complete description of the mechanism of formic acid decomposition to form $CO_{(g)}$, along with H_2O (*i.e.* dehydration) has been put forward in the recent study by Aizawa *et al.*,[129] who have used both STM and *ab initio* modelling. As already highlighted, these researchers image three formate geometries at a substrate temperature of 350 K, namely Type A, Type B, and Type C in Fig. 22. The latter two configurations involve the interaction of formate with O_b-vacs, again suggesting a role for these defects in formate decomposition. This possibility was addressed by acquisition of consecutive STM images from the same area, enabling the visualisation of dynamic processes, including conversion between different formate geometries and formate decomposition. From such images it was determined, as shown in Fig. 24, that Type C formate, which is bound in a monodentate geometry plugging an O_b-vac, decomposes. This result is consistent with Wang *et al.*'s proposal outlined above,[132] as Type C formate can be considered to be essentially equivalent to the products of reaction (7). From these

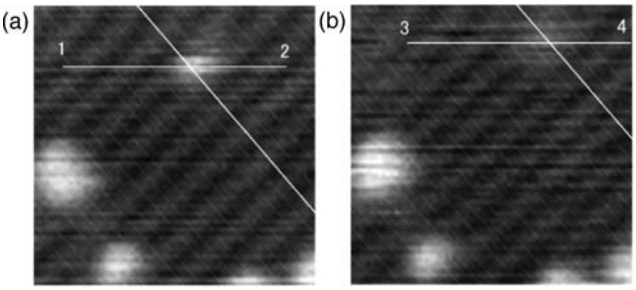

Fig. 24 Two consecutive STM images (75 Å)^2 of formate on $TiO_2(110)1\times1$ at 350 K, which Aizawa *et al.*[129] have interpreted as showing the decomposition of a Type C formate. The bright protrusion in image (a) at the intersection of the white lines is located centrally on an O_b row, and so is assigned to Type C formate. In image (b), recorded 80 s later, the brightness of this spot has significantly decreased, and it is laterally displaced along the row, which is taken as being indicative of the formate decomposing. Images are taken from ref. 129, with permission.

results, previous work, and total energy calculations, Aizawa *et al.* conclude that formic acid dehydration proceeds thus,

$$\mathrm{HCOOH}_{(g)} + \mathrm{O_b}^{2-} \rightarrow [\mathrm{HCOO}]^{-}_{(\mathrm{ads,\ Type\ A})} + \mathrm{OH_b}^{-}_{(\mathrm{ads})} \quad (8)$$

$$\mathrm{OH_b}^{-}_{(\mathrm{ads})} + \mathrm{OH_b}^{-}_{(\mathrm{ads})}, \rightarrow \mathrm{H_2O}_{(g)} + \mathrm{O_b}\text{-vac} \quad (9)$$

$$[\mathrm{HCOO}]^{-}_{(\mathrm{ads,\ Type\ A})} + \mathrm{O_b}\text{-vac} \rightarrow [\mathrm{HCOO}]^{-}_{(\mathrm{ads,\ Type\ B})} \quad (10)$$

$$[\mathrm{HCOO}]^{-}_{(\mathrm{ads,\ Type\ B})} \rightarrow [\mathrm{HCOO}]^{-}_{(\mathrm{ads,\ Type\ C})} \quad (11)$$

$$[\mathrm{HCOO}]^{-}_{(\mathrm{ads,\ Type\ C})} \rightarrow \mathrm{CO(g)} + \mathrm{OH_b}^{-}_{(\mathrm{ads})} \quad (12)$$

Given the weight of evidence to date, this is apparently a very reasonable mechanism, although further experimental effort to identify intermediates is required. Furthermore, this mechanism can operate either in the presence or absence of a partial pressure of formic acid, as no gas phase reactants are involved once the formic acid has initially adsorbed (reaction (8)). Hence, it is applicable to both the steady-state and TPD-type (*i.e.* measurements performed in vacuum) experimental scenarios.

Table 3 shows that in addition to CO, CO_2 desorbs from $TiO_2(110)$ during TPD measurements, which points to formic acid dehydrogenation (reaction (3)) occurring alongside dehydration. However, CO_2 constitutes a relatively small proportion of the desorbed products, in particular in refs. 115 and 132, indicating that dehydrogenation is not favoured. This result is consistent with Onishi *et al.*'s conclusion from steady-state measurements[114,131] that the primary channel for dehydrogenation involves a reaction between an adsorbed formate and an incoming gas phase formic acid molecule, which is not feasible under the conditions of the TPD experiments, *i.e.* there is no gas phase formic acid present. On this basis, various alternative routes, involving only adsorbed species, have been proposed, although not as yet rigorously tested, for the CO_2 production observed during TPD.[114,115,132]

Details of the bimolecular dehydrogenation reaction, which occurs under steady-state conditions, involving $[HCOO]^{-}_{(ads)}$ and $HCOOH_{(g)}$, have very recently been explored theoretically by Uemura *et al.*[133] They conclude that the dehydrogenation arises from the reaction between a Type A formate and a HCOOH molecule weakly bound to an adjacent Ti_{5c}. Interestingly, unlike the dehydration mechanism, no defect site is required, merely a series of three Ti_{5c}s.. Clearly, experimental work is required to test this theoretical prediction.

As regards decomposition of formic acid on reconstructed $TiO_2(110)$, Bennett *et al.*[130] have performed a study on the x-linked 1×2 surface with STM. They acquired images from a surface decorated with adsorbed formate whilst ramping the temperature of the substrate. Further to reduction in adsorbate density with increasing temperature, they observed formation of islands of 1×1 termination. They interpreted this phenomenon as being due to the reaction of mobile Ti^{n+} interstitials with oxygen from decomposing formate, a process well-established for high temperature O_2 exposure, as discussed in section 4.4.

5.2 Other carboxylic acids

5.2.1 Adsorption. To date, experimental evidence (*e.g.* ref. 121, 134–140) indicates that monocarboxylic acids (*i.e.* molecules with only one carboxyl group) typically mimic the room temperature adsorption of formic acid on $TiO_2(110)1\times1$, *i.e.* they form carboxylate moieties through acid hydrogen cleavage, and adopt a bonding geometry comparable to that displayed for formate in Fig. 21. Furthermore, smaller such species exhibit an ordered (2×1) overlayer at saturation (*e.g.* acetate ($[H_3CCOO]^-$),[134] propanoate ($[H_5C_2COO]^-$),[121] and trimethylacetate ($[(H_3C)_3CCOO]^-$).[136]

Concerning the fate of the acidic hydrogen, it is generally believed that it bonds to a single bridging oxygen, forming OH_b, as outlined in section 5.1.1 for formic acid. Lately, however, Lyubinetsky *et al.*[141] have challenged this perception through STM and HREELS measurements from trimethylacetate (TMA) overlayers. They interpret their STM images of isolated TMA species as indicating that the acidic hydrogen attaches to a pair of bridging oxygens rather than a single one. This bonding geometry is illustrated in Fig. 25. Given the distance between the O_bs (2.95 Å), such bonding would be rather weak, and so they propose that the hydrogen may dynamically oscillate between the two. Furthermore, they claim that the adjacent TMA is required to stabilise this geometry, and without it the hydrogen would simply bind to a single O_b, as observed following H_2O dissociation at O_b-vacs (see section 3.1). HREELS data support their hypothesis in that the O–H stretching mode expected for an OH_b is not observed on a $TiO_2(110)1\times1$ surface saturated with TMA. This rather unexpected location for the acidic hydrogen, which Lyubinetsky *et al.* conclude may pertain to other carboxylate species on $TiO_2(110)1\times1$, requires further investigation.

Studies have also been performed for the adsorption on $TiO_2(110)1\times1$ of molecules containing more than one carboxyl group. In particular, there has been interest in bi-isonicotinic acid (2,2′-bipyridine-4,4′-dicarboxylic acid), as it is the surface binding ligand in important organometallic dyes for TiO_2-based solar cells. O 1s core level PES data, acquired from $TiO_2(110)1\times1$ with a submonolayer coverage of this molecule, indicate that both –COOH groups are deprotonated and that all four oxygens are equivalent.[142] To further elucidate the adsorption geometry of this bi-isonicotinate, N K-edge NEXAFS measurements and theoretical modelling were undertaken.[142,143] A ball and stick model of the most likely adsorption geometry is displayed in Fig. 26. Recently, the

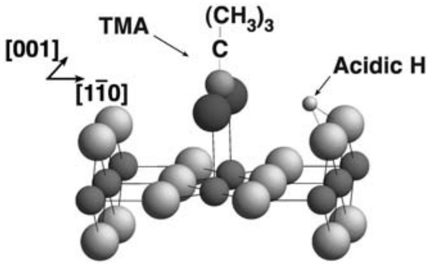

Fig. 25 Schematic diagram of Lyubinetsky *et al.*'s proposed bonding geometry[141] for the acidic hydrogen following dissociative adsorption of trimethylacetic acid on $TiO_2(110)1\times1$.

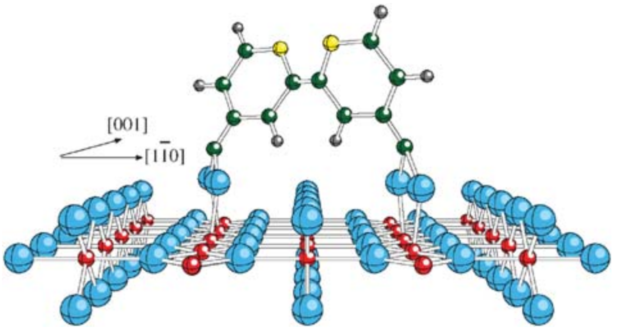

Fig. 26 Ball and stick model of the most likely adsorption geometry for bi-isonicotinate on $TiO_2(110)1\times1$ emerging from ref. 142 and 143. In the adsorbate, the light spheres in the rings are nitrogens, the dark spheres are carbons, the smallest spheres are hydrogens, and the largest are oxygen atoms.

adsorption on $TiO_2(110)1\times1$ of a complete organometallic dye molecule (Ru(4,4′-dicarboxy-2,2′-bipyridine)$_2$(NCS)$_2$), incorporating two bi-isonicotinic acid ligands, has been visualised with STM.[144] From the height of the adsorbed molecule it was deduced that it binds to the surface through two carboxylate groups, which is consistent with the work on bi-isonicotinate.[142,143] Additionally, it was found that these molecules preferentially adsorbed at step edges, which was concluded to be due to the presence of poorly coordinated Ti atoms.

As for adsorption on reconstructed $TiO_2(110)$, there has again been only limited work. Williams's group[145] have studied room temperature adsorption of acetic acid on what we assume to be the simple 1×2 phase. They conclude from valence band PES data that surface acetate is formed, binding in a similar way to acetate on the 1×1 surface, but with a saturation coverage almost half that found on the 1×1. On the grounds that their surface was comprised of Ti_2O_3 added rows, they suggest that the acetate is adsorbed on Ti_{5c} sites available in the troughs between added rows (see Fig. 5). The same group have also probed glycine (NH_2CH_2COOH) adsorption on an apparently similar 1×2 surface.[146] In this case, PES data for a submonolayer coverage adsorbed at room temperature are interpreted as indicating molecular dissociation beyond simple acidic hydrogen loss. Specifically, they conclude that the primary species on the surface is the glycine's carboxyl group, and that other components of the molecule have desorbed. Qiu and Barteau[138] have employed STM to image glycine adsorption on x-linked $TiO_2(110)1\times2$. Similar to Bennett *et al.*'s[130] STM study of formic acid on x-linked 1×2, they found no ordering of the adsorbates. From these STM images it is not possible to address the extent, if any, of glycine decomposition.

5.2.2 Thermal decomposition. Investigations into the thermal decomposition of both acetic and trimethylacetic acids on $TiO_2(110)1\times1$ have been undertaken. Onishi *et al.*[147] have examined the decomposition of the former by preparing a $(2\times1)[CH_3COO]^-$ overlayer on $TiO_2(110)$, and then acquiring a series of STM images with the substrate maintained at a temperature of 510–540 K. They observed mobile bright protrusions, which decreased in number with time. These entities were assigned to acetates undergoing decomposition. Larger immobile features, which disappeared at higher temperatures, were ascribed to carbonaceous species resulting from secondary reactions. Core level PES data recorded by Idriss *et al.*[148] also indicate the desorption of acetate in this temperature region.

The thermal decomposition of trimethylacetic acid has been studied by Henderson and co-workers,[137] employing primarily TPD. Observations largely mirror those found for formic acid on $TiO_2(110)1\times1$, as detailed previously, although additional species are desorbed due to the presence of the '$(CH_3)_3C$–'group rather than 'H–' in formic acid. TPD of an ordered (2×1) TMA overlayer, formed at 300 K, shows that CO, H_2O, and isobutene (i-C_4H_8) are all primary decomposition products. CO and isobutene (i-C_4H_8) desorb at $T_D \sim$ 660 K, along with smaller quantities of H_2O, methyl isopropenyl ketone ($CH_2{=}C(CH_3)C({=}O)CH_3$), isobutane ($i$-$C_4H_{10}$), di-*tert*-butyl ketone ($(CH_3)_3CC({=}O)C(CH_3)_3$) and/or trimethylacetic acid. The primary H_2O peak appears at $T_D \sim$ 460 K, and ^{18}O labelling measurements indicate that reaction (6) is occurring, generating O_b-vacs. Also, analogous to the thermal decomposition of adsorbed formate, these O_b-vacs are healed during TMA decomposition. Hence, a mechanism similar to the one proposed by Aizawa *et al.*[129] for the dehydration of formic acid (reactions (8)–(12)) would be consistent with these results, with the primary products, namely CO and i-C_4H_8, being produced by:

$$[(CH_3)_3CCOO]^-_{(ads,\ Type\ C)} \rightarrow CO_{(g)} + OH_b{}^-{}_{(g)} + i\text{-}C_4H_{8(g)} \qquad (13)$$

5.2.3 Photodecomposition. Motivated by interest in photocatalysis and related topics, effort has also been applied to understanding the photon induced chemistry of various organics on $TiO_2(110)$. Here, such work on acetic acid and trimethylacetic acid is discussed, the photochemistry of alcohols adsorbed on $TiO_2(110)$ being covered in section 6.2.3. Beginning with acetic acid, Idriss *et al.*[148] have examined the impact of UV radiation at room temperature on an overlayer of acetate on $TiO_2(110)1\times1$, both in UHV and in the presence O_2 ($\sim 5 \times 10^{-8}$ mbar). From C 1s core level PES spectra, it was concluded that under UHV conditions exposure to UV had no significant effect. In contrast, acetate was lost from the surface when UV illumination was performed in the partial pressure of O_2. This result was interpreted as demonstrating that UV excitation of physisorbed O_2 molecules, possibly to form $O_2{}^-{}_{(ads)}$ species, is required to initiate acetate decomposition/desorption; acetate decomposition is expected, although Idriss *et al.* do not provide any direct evidence of this process.

A more extensive study of UV photon induced chemistry has been conducted by Henderson and co-workers for trimethylacetic acid on $TiO_2(110)1\times1$.[136,149,150] First, it should be highlighted that, in contrast to Idriss *et al.*'s result for adsorbed acetate,[148] UV light does induce TMA decomposition under UHV conditions. STM images directly show that TMA coverage is depleted upon exposure to UV photons (see Fig. 27),[136] and evidence for UV driven TMA decomposition, rather than simple molecular desorption, emerges from the monitoring of gas phase species with a mass spectrometer

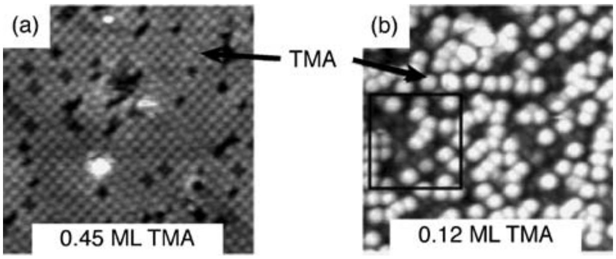

Fig. 27 STM images (160 Å)^2 of TMA covered $TiO_2(110)1\times1$ at 280 K. Image (a) shows a surface with an overlayer of 0.45 ML TMA. Image (b) shows the impact of irradiating (a) with UV light in UHV (300 W Xe arc lamp for 1 h). The TMA coverage is reduced to 0.12 ML. Images taken from ref. 136, with permission.

during irradiation. At substrate temperatures of 200 K and above, a significant amount of CO_2 is found to be evolved during such measurements, along with, once the sample is at 300 K, isobutene (i-C_4H_8) and isobutane (i-C_4H_{10}). TPD, post UV exposure, suggests that these latter two species are derived from the thermal chemistry of adsorbed *tert*-butyl radicals ($(CH_3)_3C$–), which are formed in tandem with CO_2 as a result of the primary photon driven reaction, namely TMA C–C bond cleavage giving rise to decarboxylation, *i.e.*

$$[(CH_3)_3C\text{–}COO]^-_{(ads)} + h\nu \rightarrow CO_2 + (CH_3)_3C\text{–} \quad (14)$$

Almost certainly, as is discussed in refs. 136 and 149, the photon does not directly break the C–C bond, but rather excites the TiO_2 substrate, promoting an electron from the valence band to the conduction band,

$$TiO_2 + h\nu \rightarrow e^- + h^+ \quad (15)$$

The hole (h^+) is consumed by interaction with TMA, extracting an electron from the π-system of the carboxylate group, which leads to the C–C bond breaking. It is suggested that the electron (e^-) is trapped at the surface reducing Ti^{4+} to Ti^{3+}, as is evidenced by EELS.[136]

Henderson and co-workers[149] also found that the UV induced TMA decomposition reaction was quenched much more rapidly than expected on the basis of the remaining reactant molecule density. This phenomenon was concluded to be due to the accumulation of Ti^{3+} species in the surface region, as just outlined, which interact with remaining TMA species forming Ti^{3+}–TMA entities, which are inert as regards UV decomposition. Oxidation of these Ti^{3+} species by exposing the surface to O_2 re-initiates the reaction.

Further work concerning the role of O_2 in the photodecomposition of TMA is presented by Henderson and co-workers in ref. 150. More specifically, this study focuses upon the influence of O_2 on the thermal chemistry of the *tert*-butyl radical (reaction (14)). As indicated above, this species primarily desorbs from the surface as either isobutene or isobutane. For a saturated (2×1) TMA overlayer, mass spectrometry demonstrates that, independent of O_2 partial pressure, isobutene desorption is favoured upon initial UV illumination. The lack of sensitivity to O_2 at this stage is attributed to a lack of available adsorption sites within the overlayer. As irradiation continues in UHV the isobutane yield simply increases and plateaus, producing a constant isobutene : isobutane ratio near 1 : 1. In O_2, the variation in the isobutene : isobutane ratio *versus* irradiation time is more complex. Initially, as in UHV, there is a shift towards a 1 : 1 ratio, but with time isobutene is again favoured; the precise profile is dependent upon the O_2 partial pressure. From STM of reacted surfaces it was found that the latter change can be correlated with a variation in surface morphology. Under UHV conditions, UV induced decomposition always occurs fairly randomly across the surface, whereas in O_2 extended voids appear in the TMA overlayer coinciding with the shift in selectivity back towards isobutene. Inside the voids it is concluded that adsorbed O_x species reside, and that UV induced TMA decomposition is enhanced at their borders, presumably at least partially due to O_x species removing Ti^{3+} species, with the resulting *tert*-butyl radical selectivity decomposing to isobutene. More specific reaction details remain somewhat uncertain, although it is suggested that TMA–TMA interactions may determine selectivity, and more work is required for complete atomic scale understanding. Finally, we note that the role of O_2 outlined by Henderson and co-workers is entirely different to that ascribed to it by Idriss *et al.* in the UV induced decomposition of acetate,[148] where they suppose that it directly initiates acetate bond breaking.

6. Alcohols

The reactivity of TiO_2 with alcohols is important in a number of technological applications. Methanol and ethanol, in particular, may be exploited as energy carriers in renewable sources, and alcohols in general can act as simple model contaminants to test environmental cleaning strategies, one of which is catalytic oxidation to CO_2.

In this section, we explore the dissociative and molecular adsorption of alcohols as well as various decomposition mechanisms. Methanol is discussed first, followed by a series of (C_2–C_8) aliphatic alcohols that are treated together as they share the same type of chemistry. Photodecomposition is also discussed in the case of 2-propanol and ethanol.

6.1 Methanol

6.1.1 Dissociative and molecular adsorption. TPD peaks and shoulders found for CH_3OH at ~295 K, ~350 K, and ~480 K are shown in Fig. 28.[151] Peaks are also present at ~150 K and ~165 K (off-scale in Fig. 28) which are assigned to methanol multilayers and methanol adsorbed at O_b sites, respectively. The assignment of the ~150 K peak was based on comparisons to methanol TPD from metals (*e.g.* ref. 152) whilst the ~165 K peak was assigned by analogy with the behaviour of water on $TiO_2(110)$ (section 3.3). The intense peak at ~295 K is assigned to molecular desorption of methanol adsorbed on Ti_{5c} sites, whilst the small peak at ~480 K has a coverage consistent with that of the O_b-vac density. In a SSIMS experiment analogous to the one described for water adsorption (section 3.1),[60] the $TiO(CH_3OH)^+$ signal was shown to attenuate to near zero at ~295 K with the $TiO(CH_3O)^+$ signal attenuating above ~500 K. This identifies the ~295 K peak as a molecular desorption peak and the ~480 K peak as a CH_3O/OH_{br}

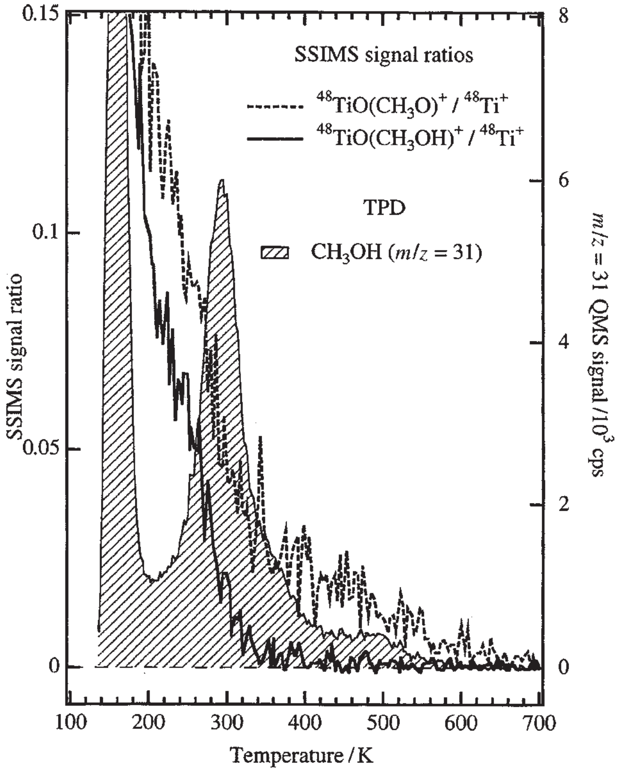

Fig. 28 Mass 31 TPD and temperature programmed SSIMS ($^{48}Ti(CH_3O)^+$ and $^{48}Ti(CH_3OH)^+$) data from multilayer CH_3OH exposed at 135 K on the $TiO_2(110)$ surface. The SSIMS data are presented as ratios with respect to the $^{48}Ti^+$ signal. In the SSIMS measurements, the Ar^+ energy was 500 eV and the current was ≤ 2 nA cm^{-2}. Reproduced with permission from ref. 151. © 1999 The Royal Society of Chemistry.

recombinative peak resulting from methanol dissociated at O_b-vacs.

When the surface is isotopically enriched with ^{18}O before exposure to $CH_3{}^{16}OH$, $CH_3{}^{16}OH$ is preferentially desorbed at ~480 K. Given the SSIMS results, the lack of isotopic scrambling of $^{18}O/^{16}O$ cannot be due to molecular desorption. Instead the isotope studies indicate that the methyl group of the methoxy is immobile, remaining attached to the ^{16}O from the dosed methanol. Therefore the recombinative desorption of methanol at ~480 K must rely on the mobility of hydrogen from OH_b.

The ~350 K peak is much more difficult to assign, with both SSIMS data and HREELS spectra being inconclusive. However, on the basis of similar behaviour following electron bombardment,[153] Henderson *et al.* tentatively assign the ~350 K peak to methanol dissociated at non-defective parts of the surface, probably Ti_{5c} sites. By combining static DFT calculations with molecular dynamics simulations, Sánchez de Armas *et al.*[154] suggest that both molecular adsorption and dissociation at Ti_{5c} sites are viable, the preferred state being highly dependent on the technical details of the calculation.

Onda *et al.*[155,156] give some indirect evidence that methanol dissociates at Ti_{5c} sites. Using 2PP spectroscopy, they detect an empty wet electron state ~2.2–2.4 eV above E_F, analogous to that found for water.[71] However, for water this state was only present when the surface had appreciable O_b-vac density, achieved by vacuum annealing. These vacancies were required in order to produce the OH_b sites associated with the wet electron state. When the surface was annealed in O_2, the wet electron state did not form. In contrast, the wet electron state forms on a methanol-exposed surface whether O_b-vacs are present or not. The different behaviour can be explained if it is not necessary for O_b-vacs to be present in order to dissociate methanol. Because of the importance of hole–electron separation in photocatalysis, it is significant that whilst electrons injected into the wet electron state associated with water decay within 15 femtoseconds,[71] wet electrons can be stabilised by methanol into the picosecond range.[156]

Zhang *et al.*[157] give direct evidence for the dissociation of methanol in O_b-vacs. Fig. 29b shows the $TiO_2(110)$ surface after a low exposure to methanol. Bright spots are observed in positions previously taken by O_b-vacs. These bright spots were assigned as methoxy and OH_b pairs, by analogy with the OH_b pairs formed from water exposure.[68] Further exposure to methanol leads to the appearance of darker spots as well as an increase in the number of bright spots (Fig. 29c). The darker spots are assigned to OH_b which have migrated along $[1\bar{1}0]$ *via* proton exchange with molecularly adsorbed methanol in a similar way to that described for water in section 3.2.[68]

Following a scan at a raised bias of +3 V, the darker spots are removed, whereas the brighter spots remain. As it has already been shown that OH_b can be removed by *ca.* +3 V tip bias, the darker species are confirmed as OH_b,[28] and the brighter spots can be assigned to methoxy groups. As the

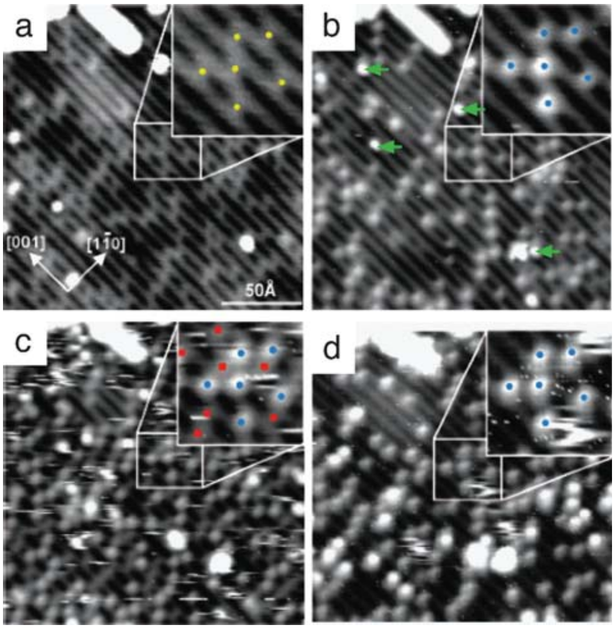

Fig. 29 STM images of same area before and after exposure of methanol on $TiO_2(110)$ at 300 K. The dosing pressure is constant in all images so the dose time is proportional to the exposure. (a) Before exposure to methanol. (b) After 80 s exposure to methanol. (c) After 110 s exposure to methanol. (d) The same area as (c) following a +3 V scan. Yellow circles show the position of O_b-vacs, blue circles show the bright features on O_b-vacs, and red squares mark the darker spots. Green arrows point at bright spots on the bright Ti_{5c} rows. Modified with permission from ref. 157.

methoxy groups take the positions of the reacting O_b-vacs, this indicates that the CH_3O–H bond is broken rather than the CH_3–OH bond.

Zhang *et al.* do not discuss whether they observe methoxy or methanol species at the Ti_{5c} sites. However, inspection of Fig. 29b, reveals the presence of a few new bright spots on the bright (Ti_{5c}) rows which may be due to either molecular methanol or methoxy dissociated at Ti_{5c} sites.

6.1.2 Decomposition.

Farfan-Arribas and Madix found a quite different behaviour in the high temperature region of their methanol TPD spectra.[158] Instead of a methanol peak at ~480 K, peaks for methanol and formaldehyde evolved at ~630 K. This discrepancy with respect to the results of Henderson *et al.* was attributed to the different sample preparation methods used. Henderson *et al.*[151] annealed their sample in UHV, as described in section 2. On the other hand, in order to assess the influence of defects on reactivity, Farfan-Arribas and Madix prepared their surfaces by first annealing, then cooling to room temperature in $\sim 2.7 \times 10^{-6}$ mbar O_2, which can lead to various surface terminations together with the presence of O_{ad}, as discussed in section 4.

When O_2 was deliberately pre-dosed onto a UHV annealed $TiO_2(110)$ surface before exposure to methanol, formaldehyde evolved at ~625 K together with methanol, regardless of the temperature of O_2 exposure (150–715 K).[151] As the mass 29 signal can have contributions from formaldehyde and methanol cracking, the mass 29 traces are scaled to the mass 31 (methanol) traces. In this way, any formaldehyde desorption shows up as the difference between the two curves as shown in Fig. 30. The partition between formaldehyde and methanol contained in the ~625 K peaks is almost equal for all O_2 exposures, suggestive of a disproportionation reaction between two methoxy groups. When O_2 is pre-exposed onto the surface at ~150 K, an additional formaldehyde shoulder evolves at low temperature (~250 K) which was attributed to a molecular O_2^- species abstracting a hydrogen atom from the methyl group of methanol.

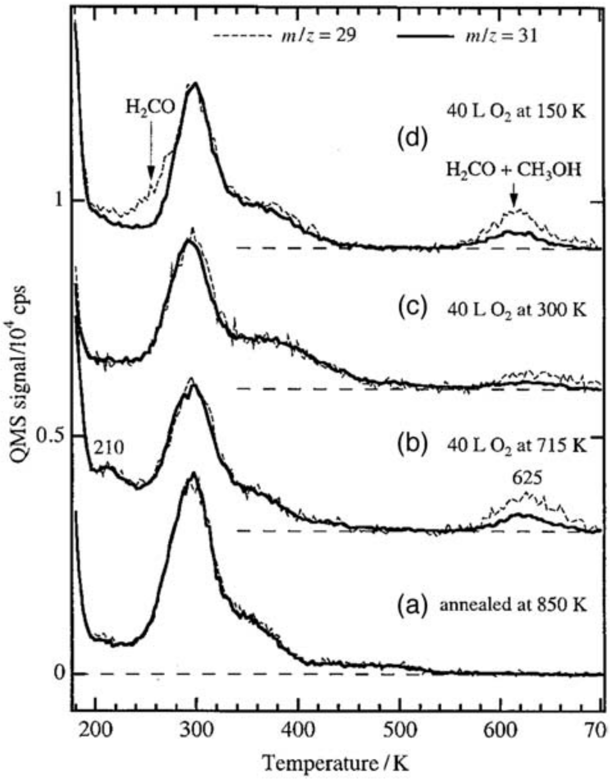

Fig. 30 The effect of O_2 pre-adsorption temperature on the TPD properties of CH_3OH from the $TiO_2(110)$ surface. TPD spectra for mass 29 (dashed lines) and mass 31 (solid lines) from a multilayer CH_3OH exposure at 135 K from: (a) the clean surface, (b) the clean surface exposed to 40 L O_2 at 715 K, (c) the clean surface exposed to 40 L O_2 at 300 K, and (d) the clean surface exposed to 40 L O_2 at 150 K. Modified with permission from ref. 151.

6.2 C_2–C_8 aliphatic alcohols

6.2.1 Dissociative and molecular adsorption.

Alcohol TPD spectra in general follow the basic pattern found for methanol in Fig. 28. Such spectra have been taken for ethanol, 2-propanol, 1-propanol, 1-butanol, 2-butanol, *tert*-butanol, 1-octanol, 2-octanol, 3-octanol, and 4-octanol.[159–165] Taking 2-propanol as an example, there is a sharp peak at ~160 K which cannot be saturated and has zero order desorption kinetics, consistent with a multilayer. Just above this is a feature tentatively assigned to 2-propanol molecules bound to the O_b atoms. Two peaks between ~250 K and ~450 K can be attributed to desorption of 2-propanol molecularly adsorbed at Ti_{5c} sites and/or recombination of OH_b and propoxy dissociated at Ti_{5c}. Finally, a high temperature peak is found at ~560 K, which becomes more intense with a greater O_b-vac density and can therefore be assigned to a recombinative reaction of propoxy at O_b-vacs and OH_b.

Zhang *et al.*[164] recorded STM images before and after exposure to 2-butanol at ~300 K. Again, in a similar way to experiments using methanol, 2-butoxy/OH_b pairs are found where O_b-vacs were previously positioned. High resolution images show that the OH_b species appear as fainter spots next to the 2-butoxy species (see Fig. 31). Isolated OH_b were also observed and attributed to OH_b which have diffused in the $[1\bar{1}0]$ direction *via* proton exchange with 2-butanol, after similar conclusions with methanol and water.[68,157] As the 2-butoxy species take the positions of the O_b-vacs filled, this indicates that, as with methanol,[157] it is the O–H bond which breaks to form the 2-butoxy species. Bright spots can also be observed on the bright Ti_{5c} rows, one of which was seen filling an O_b-vac in the sequential STM images of Fig. 31. This sequence was interpreted as molecular 2-butanol dissociating in an O_b-vac. As the adsorption behaviour of ROH, where R = H, CH_3 and 2-butyl, is similar (except for the question of whether ROH dissociates at Ti_{5c} sites where it is generally thought that there is some dissociation for alcohols at Ti_{5c} sites but not for water), Zhang *et al.* suggest that all alcohols may follow this behaviour: (i) the RO–H bond is cleaved at the O_b-vac sites with RO– taking the place of the O_b-vac and (ii) ROH adsorbs at Ti_{5c} sites and facilitates diffusion of the OH_b groups formed from dissociation at O_b-vacs.

6.2.2 Thermal decomposition.

Whilst the adsorption behaviour of alcohols in general seem to follow that of methanol, additional reaction paths are revealed when masses in addition to alcohol are tracked in TPD. One of these reactions is dehydration to alkene. Fig. 32 shows propene TPD spectra alongside traces for 2-propanol and water after $TiO_2(110)$ was exposed to mono-deuterated 2-propanol (2-PrOD). Focusing first on the high temperature (HT) region, it can be seen that the propene and 2-PrOH signals peak at ~575 K.

In an earlier study by Farfan-Arribas and Madix,[160] the 2-PrOH and equivalent 1-PrOH peaks were found ~25 K and ~40 K lower than the propene peaks, respectively. Similarly, Gamble *et al.*[162] and Farfan-Arribas and Madix,[160] respectively, found the equivalent ethanol peak ~7.5 K and ~15 K lower than the ethene peak. Farfan-Arribas and Madix also detected CO and H_2 peaks ~10–110 K higher than the alcohol peaks for 2-PrOH and 1-PrOH whereas Dohnálek and co-workers find no evidence for H_2 or CO desorption for either these or any other alcohols tested.[159,163] Different sample preparation conditions may account for the appearance of H_2 and CO in the work of Farfan-Arribas and Madix. Dohnálek and co-workers prepared their surfaces by annealing in UHV as described in section 2. Whilst Gamble *et al.* and Farfan-Arribas and Madix both annealed their samples in an O_2 pressure (1×10^{-6} and 2.7×10^{-6} mbar, respectively), Farfan-Arribas and Madix also allowed their sample to cool to room temperature in the same O_2 pressure, a procedure which we know from section 4 may lead to the formation of O_{ad}. The reason for the higher temperature onset of the alkene peaks in the earlier work is unclear, with Bondarchuk *et al.*[159] suggesting the temperature differences are within experimental error, at least for 2-propanol (and therefore implicitly for ethanol where the temperature offset is less).

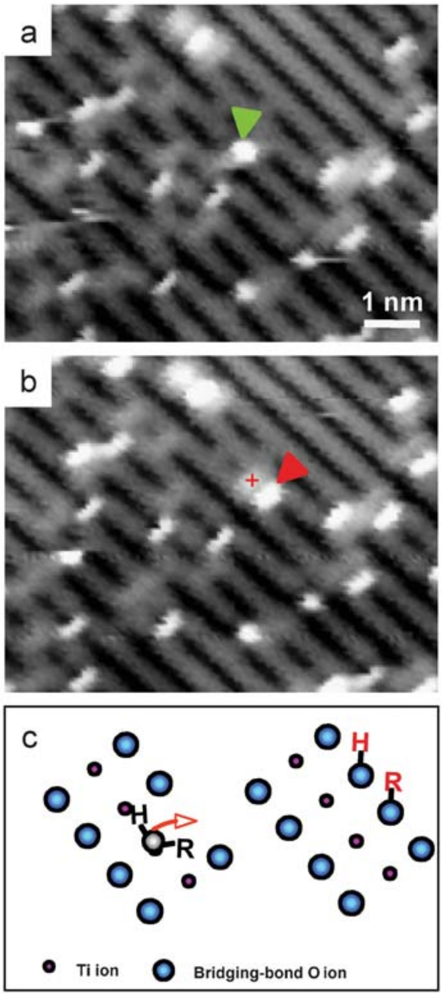

Fig. 31 Sequential STM images showing a 2-butanol molecule initially adsorbed on a Ti_{5c} site dissociating at an O_b-vac. (a) Before dissociation, the 2-butanol molecule is indicated with a green arrowhead. (b) After the reaction, the 2-butoxy takes the position of the O_b-vac (red arrowhead) and the OH_b sits adjacently (red cross). (c) Schematic representation of the dissociation process. Modified from ref. 164 with permission.

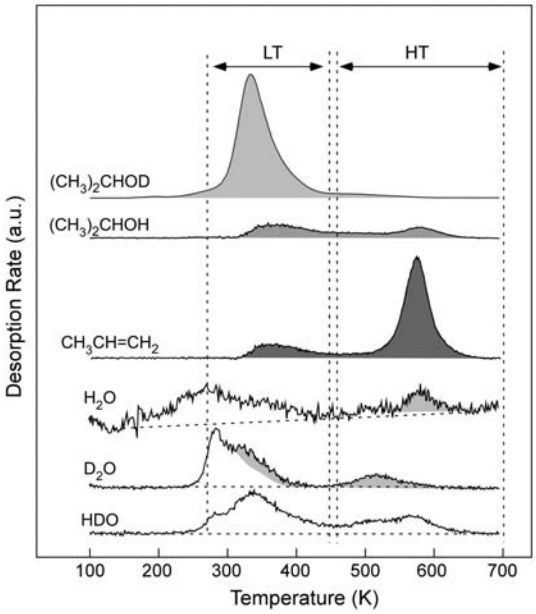

Fig. 32 TPD profiles of dehydration products from 0.45 ML mono-deuterated 2-propanol (2-PrOD) dosed on $TiO_2(110)$ at 100 K. The surface contains a density of 0.035 ML O_b-vacs. Contributions from fragmentation of 2-PrOD traced by mass 46 have been subtracted from the mass 18, 19, 20, 41, and 45 curves to obtain the net desorption profiles of H_2O, HDO, D_2O, C_3H_6, and $(CH_3)_2CHOH$, respectively. Shaded regions correspond to the desorption of reactants and products from $TiO_2(110)$. The unshaded regions in the HDO and H_2O spectra are affected by experimental artefacts and cannot be unambiguously assigned. Modified from ref. 163 with permission.

Returning to Fig. 32: the ~575 K propene and 2-PrOH peaks are sandwiched by two water peaks—one ~60 K below at ~515 K, the other ~5 K higher at ~580 K. The water peak at ~515 K is well understood and arises from the recombination of two OH_b groups (see section 3.1 for further details and notice that due to an offset of the temperature scale compared with the earlier work, the peak is slightly shifted from ~490 K). In Fig. 32, this ~515 K water peak is dominated by D_2O and must therefore arise from OD_b formed from dissociated 2-PrOD. The propene evolved from 2-PrOD is always C_3H_6, ruling out any mechanism which incorporates the O–H hydrogen into the resulting alkene. For ethanol, Gamble *et al.*[162] then Kim *et al.*[165] tested the dehydration mechanism by using CD_3CH_2OH, with the product always being CD_2CH_2. This is a key result because it shows that it is the C2 carbon–hydrogen bond that is eliminated.

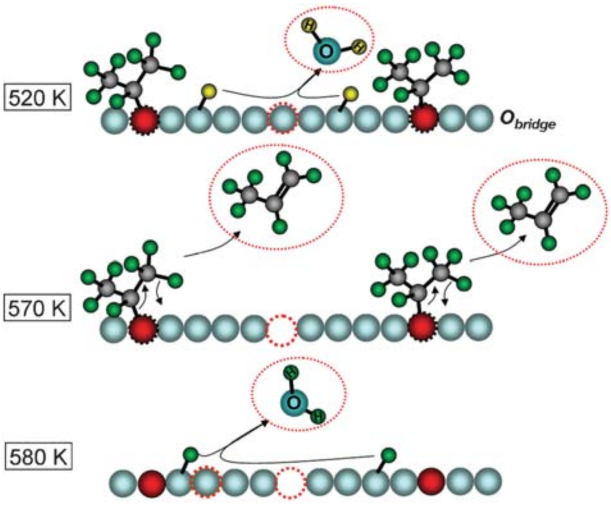

Fig. 33 Schematic representation of the proposed reaction mechanism of 2-propoxy and hydroxyl groups at high temperature (> 500 K). The red circles denote original positions of O_b-vacs which are filled with the oxygen from 2-propoxy when 2-propanol dissociates. The yellow circles represent the hydrogen which forms the accompanying OH_b species. At 520 K, the hydrogens are mobile along the O_b rows and can react to form water that desorbs leaving a new O_b-vac (blue circle with a dashed red outline). At 570 K, 2-propoxy groups react by dehydration to form propene by C2–H and C1–O_b bond breaking. This leaves further OH_b groups with an increasing concentration as propene forms and as these OH_b react together, the second water desorption peak forms. Reproduced from ref. 159 with permission. © 2007 American Chemical Society.

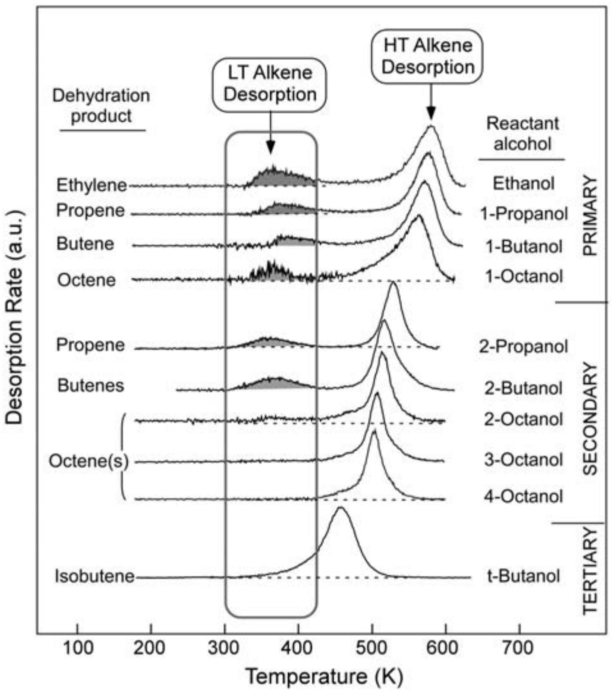

Fig. 34 TPD spectra of alkene formation from 10 alcohols dosed on $TiO_2(110)$ at 100 K. The spectra are grouped as primary, secondary, and tertiary alcohols. The net alkene desorption spectra shown were obtained by subtracting the fragmentation contributions of molecular alcohol. Mass 27 and 41 were used for ethene and propene, respectively, and mass 56 was used for butenes and octenes. The alcohol dose in each case was that which saturates the O_b-vacs and the Ti_{5c} sites. All spectra were normalized to the HT alkene desorption peaks. The surface in each case contained a density of 0.035 ML O_b-vacs before exposure to alcohol. Modified from ref. 163 with permission.

There are other notable isotope effects. When 2-PrOD$_8$ is used, the propene peak is found ~10 K higher than when either 2-PrOH or 2-PrOD is used. This indicates that C–H (or C–D) bond stretching is involved in the rate-determining step for propene formation. Likewise, in the earlier ethanol study,[162] CD_3CH_2OH gave an ethene peak ~8.5 K higher than CH_3CH_2OD, showing specifically that it is the C2 carbon–hydrogen bond which is involved in the rate-determining step.

The HT dehydration mechanism proposed by Bondarchuk *et al.*[159] is shown in Fig. 33 using 2-propanol as an example. As the temperature increases, a hydrogen atom connected to the C2 carbon forms a bond with an O_b atom so that the 2-propoxy thermally passes through a cyclic activated complex (O_b–C–C–H–O_b) that concertedly leads to the formation of propene and OH_b. The evolved OH_b recombines either with a propoxy to form 2-PrOH or another OH_b to form H_2O. These two reactions explain the desorption of non-deuterated 2-PrOH at ~575 K and water at ~580 K, when 2-PrOD is used as in Fig. 32. Conversely, when the surface was exposed to 1-C_3D_7OH,[160] fully-deuterated 1-propanol desorbs in this HT peak.

Alkyl substituents display an inductive effect whereby electron density is released to carbon atoms connected to electronegative atoms. Larger R groups have a greater inductive effect, as do multiple R groups. By investigating the peak desorption temperatures for a number of alcohols, Kim *et al.*[165] showed that alcohols with more inductive R groups convert to the alkene at lower temperatures. In line with this, Fig. 34 shows that the temperature of the HT alkene peaks increases from tertiary to secondary, and finally to primary alcohols. They concluded that the induction stabilises the C1 carbon$^{\delta+}$–O_b bond in their proposed cyclic complex, thereby reducing the activation energy for alkene formation. This dependence on the inductive effect gives evidence for heterolytic bond cleavage during the dehydration of these alcohols and therefore conflicts with a radical mechanism proposed by Farfan-Arribas and Madix.[160] Furthermore, the observation that both C1 carbon–O_b elongation and C2 carbon–H stretching affects the TPD peak positions indicates that both are involved in the rate-determining step, in line with the cyclic complex proposed.[159]

We turn now to the low temperature (LT) region in Fig. 32 where it is apparent that propene is also produced.[159,163] This is consistent with the TPD results of Gamble *et al.* where an ethene peak evolved from ethanol TPD at ~360 K as well as ~650 K.[162] Kim *et al.*[163] showed that alkene evolution in this temperature range is not affected by the presence of O_b-vacs. This was tested by pre-dosing the $TiO_2(110)$ with water in order to fill the O_b-vacs with OH_b. This suppressed the HT alkene channel but in the LT region, propene TPD spectra were identical to those recorded without water pre-dosing. There are two significant features of the LT TPD region in Fig. 32: (1) a 2-PrOH peak appears at a similar temperature to the LT propene peak, which is surprising because the alcohol dosed was 2-PrOD; (2) a broad D_2O feature appears between ∼250–400 K with local peaks at ∼290 K and ∼330 K. The lower temperature peak at ∼290 K corresponds to molecular desorption of water adsorbed at Ti_{5c} sites (see section 3.1 and notice that the equivalent peak was found at ∼265 K due to systematic offset in the temperatures) but the origin of the peak at ∼330 K is unknown.

Fig. 34 shows the LT channel is open for 7 of the 10 alcohols tested, the exceptions being for 3-octanol, 4-octanol, and *tert*-butanol. From this, Kim *et al.*[163] suggest that for the LT channel to proceed, one R group must be hydrogen and one of the other R groups must either be hydrogen again or CH_3.

The tentative reaction mechanism proposed by Kim *et al.*[163] and illustrated in Fig. 35 can explain all these observations. The reaction involves one alcohol and one alkoxy both adsorbed on Ti_{5c} sites randomly meeting with a specific orientation. Using 2-PrOD as an example, 2-propoxy abstracts H from the 2-propoxy group of 2-PrOD explaining the desorption of non-deuterated 2-PrOH. The previously adsorbed 2-PrOD which has lost its H atom to the 2-propoxy rearranges and desorbs as propene, leaving behind an OD group attached to Ti_{5c} (OD_t). This OD_t group can then recombine with OD_b (already formed by dissociation of 2-PrOD at either Ti_{5c} sites or O_b-vacs) so there is no net loss or gain of O at the surface. Desorption of D_2O thus formed could be responsible for the peak at ∼330 K, which seems reasonable given that OH_t groups recombine with each other at ∼290–320 K (see sections 4.1 and 4.3). The requirement for the alcohol and alkoxy to meet in a specific orientation accounts for the fact that the bulkier alcohols do not form alkenes in the LT region.

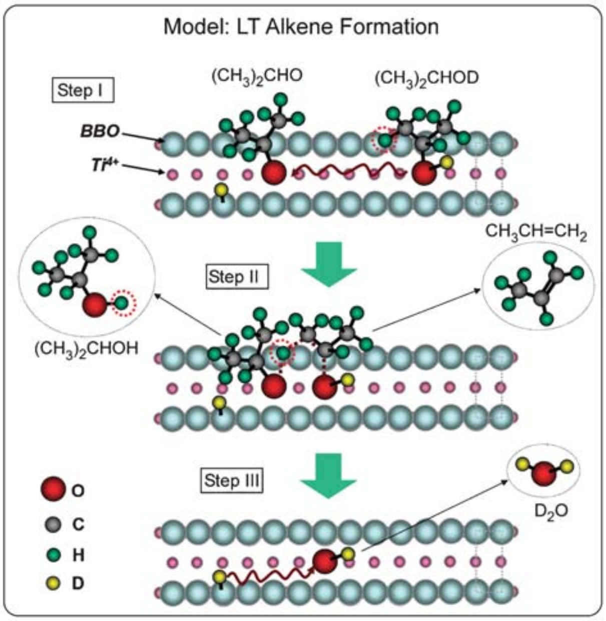

Fig. 35 Schematic of proposed LT dehydration mechanism. The key intermediate is a complex (step II) formed by interaction of an oriented alkoxy with an oriented chemisorbed alcohol (step I). There is a concerted rearrangement that involves a C2 hydrogen coupling to the alkoxy oxygen and simultaneous cleavage of the C–O bond of the chemisorbed alcohol. Step III illustrates the final recombinative desorption of D_2O. Reproduced from ref. 163 with permission. © 2007 American Chemical Society.

There is another HT pathway active only for some of the alcohols studied, namely dehydrogenation to the corresponding aldehyde. As described in section 6.1.2, for aldehyde TPD spectra, masses with contributions from both the parent alcohol and the aldehyde are tracked. These are scaled and superimposed on traces from the parent alcohol. In this way, the difference between the curves corresponds to the aldehyde yield. Following this procedure, Kim *et al.*[163] show that aldehydes evolve at about the same temperature as the corresponding HT alcohol desorption peak. As such, dehydrogenation was attributed to alkoxy adsorbed at the O_b-vacs.

Aldehyde formation has only been observed for primary alcohols.[160,163] Based on the assumption that a hydrogen atom is abstracted directly from the C1 carbon to form aldehyde, this selection rule can be quite simply understood. Tertiary alcohols can be excluded immediately because they have no such hydrogen species by definition. Assuming that the two C1–H bonds are equivalent in primary alcohols, then the probability for dehydrogenation of primary alcohols, based only on the presence of two C1 hydrogen atoms rather than one, must be twice that of secondary alcohols. Added to this, it has already been shown that the activation energy for dehydration of secondary alcohols is lower than for primary alcohols. Hence, for secondary alcohols, dehydrogenation will compete less successfully against dehydration than it would for primary alcohols.

Kim *et al.*[163] found the aldehyde yield to be much smaller than the alkene and alcohol yields for the alcohols tested. For example, the propanal yield from 1-propanol was about 10% of the HT propene yield. In the case of ethanol, Gamble *et al.*[162] did not detect any significant amount of acetaldehyde, presumably because the signal was too weak. On the other hand, Farfan-Arribas and Madix[160] found an equal three-way partition of alcohol, alkene, and aldehyde in the HT region for both ethanol and 1-propanol. As discussed for the formation of CO, this divergence from the results of Gamble *et al.* and Kim *et al.* may be due to differences in sample preparation.

6.2.3 Photodecomposition.

Using molecular beam studies, Brinkley and Engel found a new dehydrogenation pathway for 2-propanol.[166,167] A mixed beam of O_2 and 2-propanol in a 7 : 1 ratio was directed at the $TiO_2(110)$ surface which was then irradiated with UV light. When the light was switched on, a mass spectrometer detected intense transient peaks for acetone and water, both of which decayed in seconds then remained constant until the light was switched off. The transient peaks are due to the surface being saturated with O_2 and 2-propanol in the interval before the light was switched on. This leads to a rapid initial reaction when the light is first switched on, but once the excess O_2 and 2-propanol are consumed in the production of acetone, the reaction becomes limited by the molecular beam flux and the curves fall to steady-state levels. The acetone and water yields are approximately equal, suggesting that one 2-propanol molecule reacts with half an O_2 molecule to form one acetone molecule and one water molecule.

The same reaction was also performed 'statically'. In this case, the same 2-propanol–O_2 mixture was beamed onto a $TiO_2(110)$ surface held at ~185 K, after which the surface was irradiated with UV light with the molecular beam switched off. Any adsorbates were then desorbed into a mass spectrometer to measure the total amount of acetone produced, which maximised at ~0.17 ML. On a fully oxidised surface, prepared by annealing in 1.3×10^{-6} mbar O_2 then cooling in the same O_2 pressure to 300 K, the maximum amount of acetone produced fell to ~0.08 ML, but did not reduce completely. This led Brinkley and Engel to conclude that about half of the acetone originated from 2-propanol somehow associated with O_b-vacs, with the other half coming from 2-propanol at other defect sites, such as step edges. O_b-vacs were not thought to participate directly in the reaction because the oxidising conditions of the experiment would fill them. Given what is now known about the behaviour of O_2 on $TiO_2(110)$ (see section 4), the importance of the O_b-vacs may lie in facilitating the formation of O_{ad} species. Brinkley and Engel suggest that photoexcited electrons are captured by O_2, thus allowing the holes (h^+) to attack the 2-propanol molecules and initiate dehydrogenation to acetone.

By tracking the C 1s peaks using core level PES, Jayaweera *et al.*[168] monitored the effect of UV illumination on ethanol adsorbed on $TiO_2(110)$. A small peak evolved at ~290 eV that was attributed to either acetate or formate anions. When the same procedure is followed in a pressure of 1.3×10^{-6} mbar O_2, a much clearer ~290 eV peak developed. Thus the reaction on the clean surface was attributed to background O_2, the clean surfaces being prepared by annealing in 6.7×10^{-5} mbar O_2. By comparison with work on powdered TiO_2,[169] Jayaweera *et al.* conclude that the first step in the reaction is dehydrogenation to acetaldehyde, after which further oxidation forms either acetate or formate, with CO_2 being released in the latter case. The initial step in the mechanism proposed by Jayaweera *et al.* is the same as that proposed by Brinkley and Engel, *i.e.* O_2 captures photoexcited electrons.[167] However, the next step in Jayaweera *et al.*'s proposed mechanism differs in that they envisage a direct reaction between ethoxy and O_2^-. Further work is needed in order to achieve an atomic level understanding of both these photoreactions.

7. Outlook

Whilst not yet approaching our level of understanding of metal surfaces, our knowledge of oxide surface chemistry has developed considerably over the last decade or so. This is especially so in the case of the model oxide surface $TiO_2(110)$, where trends are clearly emerging that are quite different to the behaviour of metals. In particular, the role of defects such as O vacancies has now been evaluated in exquisite detail and it is clear that they play a crucial role in surface reactions. This evaluation has involved the application of scanning probe methods in combination with first principles calculations, both of which have followed mechanistic studies using 'conventional' methods.

There is a clear need to further extend the surface reaction studies to other types of metal oxide surface in order to evaluate trends in reaction mechanisms across different oxide surfaces. Iron oxides would be good initial candidates since Fe_2O_3 is a promising catalyst, for instance in the oxidation of benzene and chlorobenzene, and various Fe_xO_y compounds play an important role in geochemistry. Of course, there have been a number of surface chemistry studies of metal oxide surfaces other than $TiO_2(110)$, including those of iron oxides, but very few of these match the mechanistic detail demonstrated in this review.

In the near future there is no doubt that a lot of attention will be focused on studies at elevated pressures and at the solid–liquid interface. Photon-in photon-out techniques, such as SXRD, will be employed, as well as approaches modified to operate in the high pressure regime, *e.g.* high-pressure PES, which has already been applied to the $TiO_2(110)1\times1$/water system.[87,88] An area of particular topical interest is the interface between light harvesting surfaces (*e.g.* TiO_2) and liquid water in connection with photocatalysis. Ultra-fast timing measurements may also have a significant impact here. It might be possible to use pump probe measurements, involving a UV pump and soft X-ray probe to look at charge transfer processes following the light harvesting event. It has already proved possible to measure the 15 fs lifetime of a 'wet electron state' on $TiO_2(110)$ using two-photon photoemission.[71]

Material in this review highlights the enormous impact that scanning probe methods have had on our understanding of reactions at oxide surfaces. However, the lack of chemical specificity with STM and AFM is a limitation. STM-inelastic electron tunnelling spectroscopy could be a solution; this is a technique that can be used to measure the vibrational spectrum of a single molecule.[170,171] Another technique that can be used to image with chemical specificity is X-ray photoelectron microscopy.[172,173] Although this is currently limited to a spatial resolution of 20 nm or so, it is hoped that this will improve to 2 nm over the next decade. Realising this goal would open new vistas.

References

1 M. Grätzel, *Nature (London)*, 2001, **414**, 338.
2 H. Imagawa, T. Tanaka, N. Takahashi, S. Matsunaga, A. Suda and H. Shinjoh, *J. Catal.*, 2007, **251**, 315.
3 A. Fujishima, T. N. Rao and D. A. Tyrk, *J. Photochem. Photobiol., C*, 2000, **1**, 1.
4 R. Blossey, *Nat. Mater.*, 2003, **2**, 301.
5 B. Karunagaran, P. Uthirakumar, S. J. Chung, S. Velumani and E.-K Suh, *Mater. Charact.*, 2007, **58**, 680.
6 F. H. Jones, *Surf. Sci. Rep.*, 2001, **42**, 75.
7 G. X. Shen, R. G. Du, Y. C. Chen, C. J. Lin and D. J. Scantlebury, *Corrosion*, 2005, **61**, 943.
8 K. C. Popat, M. Eltgroth, T. J. La Tempa, C. A. Grimes and T. A. Desai, *Small*, 2007, **3**, 1878.
9 A. J. Limb, O. Bikondoa, C. A. Muryn and G. Thornton, *Angew. Chem., Int. Ed.*, 2007, **46**, 549.
10 http://nobelprize.org/nobel_prizes/chemistry/laureates/2007/.
11 U. Diebold, *Surf. Sci. Rep.*, 2003, **48**, 53.
12 G. Charlton, P. B. Howes, C. L. Nicklin, P. Steadman, J. S. G. Taylor, C. A. Muryn, S. P. Harte, J. Mercer, R. McGrath, D. Norman, T. S. Turner and G. Thornton, *Phys. Rev. Lett.*, 1997, **78**, 495.
13 B. Hird and R. A. Armstrong, *Surf. Sci.*, 1999, **420**, L131.
14 E. Asari, T. Suzuki, H. Kawanowa, J. Ahn, W. Hayami, T. Aizawa and R. Souda, *Phys. Rev. B*, 2000, **61**, 5679.

15 R. Lindsay, A. Wander, A. Ernst, B. Montanari, G. Thornton and N. M. Harrison, *Phys. Rev. Lett.*, 2005, **94**, 246102.

16 G. S. Parkinson, M. A. Muñoz-Márquez, P. D. Quinn, M. J. Gladys, R. E. Tanner, D. P. Woodruff, P. Bailey and T. C. Q. Noakes, *Phys. Rev. B*, 2006, **73**, 245409.

17 E. A. Kröger, D. I. Sayago, F. Allegretti, M. J. Knight, M. Polcik, W. Unterberger, T. J. Lerotholi, K. A. Hogan, C. L. A. Lamont and D. P. Woodruff, *Phys. Rev. B*, 2007, **75**, 195413.

18 G. Cabailh, X. Torrelles, R. Lindsay, O. Bikondoa, I. Joumard, J. Zegenhagen and G. Thornton, *Phys. Rev. B*, 2007, **75**, 241403(R).

19 V. Swamy, J. Muscat, J. D. Gale and N. M. Harrision, *Surf. Sci.*, 2002, **504**, 115.

20 A. Kiejna, T. Pabisiak and S. W. Gao, *J. Phys.: Condens. Matter*, 2006, **18**, 4207.

21 S. J. Thompson and S. P. Lewis, *Phys. Rev. B*, 2006, **73**, 073403.

22 K. J. Hameeuw, G. Cantele, D. Ninno, F. Trani and G. Iadonisi, *J. Chem. Phys.*, 2006, **124**, 024708.

23 F. Labat, P. Baranek and C. Adamo, *J.Chem. Theory Comput.*, 2008, **4**, 341.

24 U. Diebold, J. F. Anderson, K.-O. Ng and D. Vanderbilt, *Phys. Rev. Lett.*, 1996, **77**, 1322.

25 H. Onishi, K. Fukui and Y. Iwasawa, *Bull. Chem. Soc. Jpn.*, 1995, **68**, 2447.

26 S. Fischer, A. W. Munz, K.-D. Schierbaum and W. Göpel, *Surf. Sci.*, 1995, **337**, 17.

27 K. Fukui, H. Onishi and Y. Iwasawa, *Phys. Rev. Lett.*, 1997, **79**, 4202.

28 O. Bikondoa, C. L. Pang, R. Ithnin, C. A. Muryn, H. Onishi and G. Thornton, *Nat. Mater.*, 2006, **5**, 189.

29 T. L. Thompson, O. Diwald and J. T. Yates, *J. Phys. Chem. B*, 2003, **107**, 11700.

30 Z. Zhang, S.-P. Jeng and V. E. Henrich, *Phys. Rev. B*, 1991, **43**, 12004.

31 A. G. Thomas, W. R. Flavell, A. K. Mallick, A. R. Kumarasinghe, D. Tsoutsou, N. Khan, C. Chatwin, S. Rayner, G. C. Smith, R. L. Stockbauer, S. Warren, T. K. Johal, S. Patelm D. Holland, A. Taleb and F. Wiame, *Phys. Rev. B*, 2007, **75**, 035105.

32 S. Krischok, J. Günster, D. W. Goodman, O. Höfft and V. Kempter, *Surf. Interface Anal.*, 2004, **36**, 77.

33 R. L. Kurtz, R. Stockbauer, T. E. Madey, E. Román and J. L. De Segovia, *Surf. Sci.*, 1989, **218**, 178.

34 M. A. Henderson, W. S. Epling, C. H. F. Peden and C. L. Perkins, *J. Phys. Chem. B*, 2003, **107**, 534.

35 L. Q. Wang, A. N. Shultz, D. R. Baer and M. H. Engelhard, *J. Vac. Sci. Technol., A*, 1996, **14**, 1532.

36 K. Onda, B. Li and H. Petek, *Phys. Rev. B*, 2004, **70**, 045415.

37 P. Krüger, S. Bourgeois, B. Domenichini, H. Magnan, D. Chandesris, P. Le Fèvre, A. M. Flank, J. Jupille, L. Floreano, A. Cossaro, A. Verdini and A. Morgante, *Phys. Rev. Lett.*, 2008, **100**, 055501.

38 M. Li, W. Hebenstreit, U. Diebold, A. M. Tyryshkin, M. K. Bowman, G. G. Dunham and M. A. Henderson, *J. Phys. Chem. B*, 2000, **104**, 4944.

39 P. J. Møller and M.-C. Wu, *Surf. Sci.*, 1989, **224**, 265.

40 H. Onishi and Y. Iwasawa, *Surf. Sci.*, 1994, **313**, L783.

41 H. Onishi and Y. Iwasawa, *Phys. Rev. Lett.*, 1996, **76**, 791.

42 C. L. Pang, S. A. Haycock, H. Raza, P. W. Murray, G. Thornton, O. Gülersen, R. James and D. W. Bullett, *Phys. Rev. B*, 1998, **58**, 1586.

43 C. L. Pang, H. Raza, S. A. Haycock and G. Thornton, *Appl. Surf. Sci.*, 2000, **157**, 233.

44 K. T. Park, M. H. Pan, V. Meunier and E. W. Plummer, *Phys. Rev. Lett.*, 2006, **96**, 226105.

45 M. Blanco-Rey, J. Abad, C. Rogero, J. Méndez, M. F. López, J. A. Martín-Gago and P. L. Andrés, *Phys. Rev. Lett.*, 2006, **96**, 055502.

46 M. Blanco-Rey, J. Abad, C. Rogero, J. Méndez, M. F. López, E. Román, J. A. Martín-Gago and P. L. Andrés, *Phys. Rev. B*, 2007, **75**, 081402(R).

47 Q. Guo, I. Cocks and E. M. Williams, *Phys. Rev. Lett.*, 1996, **77**, 3851.

48 E. Asari and R. Souda, *Phys. Rev. B*, 1999, **60**, 10719.

49 S. D. Elliot and S. P. Bates, *Phys. Rev. B*, 2002, **65**, 245415.

50 S. D. Elliot and S. P. Bates, *Phys. Rev. B*, 2003, **67**, 035421.

51 R. A. Bennett, P. Stone, N. J. Price and M. Bowker, *Phys. Rev. Lett.*, 1999, **82**, 3831.

52 S. Takakusagi, K. Fukui, F. Nariyuki and Y. Iwasawa, *Surf. Sci.*, 2003, **523**, L41.

53 X. Torrelles, G. Cabailh, W. Busayaporn, A. Wander, N. M. Harrison, G. Thornton, O. Bikondoa, I. Joumard, J. Zegenhagen and R. Lindsay, unpublished work.

54 P. W. Murray, N. G. Condon and G. Thornton, *Phys. Rev. B*, 1995, **51**, 10989.

55 M. A. Henderson, *Surf. Sci. Rep.*, 2002, **46**, 1.

56 P. Maksymovych, S. Mezhenny and J. T. Yates, Jr, *Chem. Phys. Lett.*, 2003, **382**, 270.

57 M. B. Hugenschmidt, L. Gamble and C. T. Campbell, *Surf. Sci.*, 1994, **302**, 329.

58 M. A. Henderson, *Surf. Sci.*, 1996, **355**, 151.

59 M. A. Henderson, *Langmuir*, 1996, **12**, 5093.

60 M. A. Henderson, *Surf. Sci.*, 1998, **400**, 203.

61 C. Di Valentin, G. Pacchioni and A. Selloni, *Phys. Rev. Lett.*, 2006, **97**, 166803.

62 I. M. Brookes, C. A. Muryn and G. Thornton, *Phys. Rev. Lett.*, 2001, **87**, 266103.

63 S. Suzuki, K. Fukui, H. Onishi and Y. Iwasawa, *Phys. Rev. Lett.*, 2000, **84**, 2156.

64 R. Schaub, P. Thostrup, N. Lopez, E. Laegsgaard, I. Stensgaard, J. K. Nørskov and F. Besenbacher, *Phys. Rev. Lett.*, 2001, **87**, 266104.

65 C. L. Pang, O. Bikondoa, D. S. Humphrey, A. C. Papageorgiou, G. Cabailh, R. Ithnin, Q. Chen, C. A. Muryn, H. Onishi and G. Thornton, *Nanotechnology*, 2006, **17**, 5397.

66 G. Teobaldi, W. A. Hofer, O. Bikondoa, C. L. Pang, G. Cabailh and G. Thornton, *Chem. Phys. Lett.*, 2007, **437**, 73.

67 S. Wendt, R. Schaub, J. Matthiesen, E. K. Vestergaard, E. Wahlström E, M. D. Rasmussen, P. Thostrup, L. M. Molina, E. Lægsgaard, I. Stensgaard, B. Hammer and F. Besenbacher, *Surf. Sci.*, 2005, **598**, 226.

68 S. Wendt, J. Matthiesen, R. Schaub, E. K. Vestergaard, E. Lægsgaard, F. Besenbacher and B. Hammer, *Phys. Rev. Lett.*, 2006, **96**, 066107.

69 Z. Zhang, O. Bondarchuk, B. D. Kay J. M. White and Z. Dohnálek, *J. Phys. Chem. B*, 2006, **110**, 21840.

70 U. Diebold, J. Lehman, T. Mahmoud, M. Kuhn, G. Leonardelli, W. Hebenstreit, M. Schmid and P. Varga, *Surf. Sci.*, 1998, **411**, 137.

71 K. Onda, B. Li, J. Zhao, K. D. Jordan, J. Yang and H. Petek, *Science*, 2005, **308**, 1154.

72 C. Di Valentin, *J. Chem. Phys.*, 2007, **127**, 154705.

73 C. L. Pang, A. Sasahara, H. Onishi, Q. Chen and G. Thornton, unpublished.

74 C. L. Pang, A. Sasahara, H. Onishi, Q. Chen and G. Thornton, *Phys. Rev. B*, 2006, **74**, 073411.

75 J. V. Lauritsen, A. S. Foster, G. H. Olesen, M. C. Christensen, A. Kühnle, S. Helveg, J. R. Rostrup-Nielsen, B. S. Clausen, M. Reichling and F. Besenbacher, *Nanotechnology*, 2006, **17**, 3436.

76 G. H. Enevoldsen, A. S. Foster, M. C. Christensen, J. V. Lauritsen and F. Besenbacher, *Phys. Rev. B*, 2007, **76**, 205415.

77 R. Schaub, E. Wahlström, A. Rønnau, E. Lægsgaard, I. Stensgaard and F. Besenbacher, *Science*, 2003, **299**, 377.

78 R. Schaub, *Science*, 2006, **314**, 5801.

79 T. L. Thompson, O. Diwald and J. T. Yates, Jr, *Chem. Phys. Lett.*, 2004, **393**, 28.

80 F. Allegretti, S. O'Brien, M. Polcik, D. I. Sayago and D. P. Woodruff, *Phys. Rev. Lett.*, 2005, **95**, 226104.

81 F. Allegretti, S. O'Brien, M. Polcik, D. I. Sayago and D. P. Woodruff, *Surf. Sci.*, 2006, **600**, 1487.

82 E. V. Stefanovich and T. T. Truong, *Chem. Phys. Lett.*, 1999, **299**, 623.

83 C. Zhang and P. J. D. Lindan, *J. Chem. Phys.*, 2004, **121**, 3811.

84 P. A. Thiel and T. E. Madey, *Surf. Sci. Rep.*, 1987, **7**, 211.

85 N. G. Petrik and G. A. Kimmel, *Phys. Rev. Lett.*, 2007, **99**, 196103.

86 C. D. Lane, N. G. Petrik, T. M. Orlando and G. A. Kimmel, *J. Phys. Chem. C*, 2007, **111**, 16319.

87 G. Ketteler, S. Yamamoto, H. Bluhm, K. Andersson, D. E. Starr, D. F. Ogletree, H. Ogasawara, A. Nilsson and M. Salmeron, *J. Phys. Chem. C*, 2007, **111**, 8278.

88 S. Yamamoto, H. Bluhm, K. Andersson, G. Ketteler, H. Ogasawara, M. Salmeron and A. Nilsson, *J. Phys.: Condens. Matter*, 2008, **20**, 184025.
89 J. M. Pan, B. L. Maschhoff, U. Diebold and T. E. Madey, *J. Vac. Sci. Technol., A*, 1992, **10**, 2470.
90 C. L. Perkins and M. A. Henderson, *J. Phys. Chem. B*, 2001, **105**, 3856.
91 W. S. Epling, C. H. F. Peden, M. A. Henderson and U. Diebold, *Surf. Sci.*, 1998, **412/413**, 333.
92 M. D. Rasmussen, L. M. Molina and B. Hammer, *J. Chem. Phys.*, 2004, **120**, 988.
93 X. Wu, A. Selloni, M. Lazzeri and S. K. Nayak, *Phys. Rev. B*, 2003, **68**, 241402(R).
94 Y. Du, Z. Dohnálek and I. Lyubinetsky, *J. Phys. Chem. C*, 2008, **112**, 2649.
95 U. Diebold, W. Hebenstreit, G. Leonardelli, M. Schmid and P. Varga, *Phys. Rev. Lett.*, 1998, **81**, 405.
96 M. A. Henderson, W. S. Epling, C. L. Perkins, C. H. F. Peden and U. Diebold, *J. Phys. Chem. B*, 1999, **103**, 5328.
97 G. Lu, A. Linsebigler and J. T. Yates, Jr, *J. Chem. Phys.*, 1995, **102**, 4657.
98 C. N. Rusu and J. T. Yates, Jr, *Langmuir*, 1997, **13**, 4311.
99 T. L. Thompson and J. T. Yates, Jr, *J. Phys. Chem. B*, 2006, **110**, 7431.
100 T. L. Thompson and J. T. Yates, Jr, *Top. Catal.*, 2005, **35**, 197.
101 T. L. Thompson and J. T. Yates, Jr, *Chem. Rev.*, 2006, **106**, 4428.
102 R. Kopelman, *J. Stat. Phys.*, 1986, **42**, 185.
103 A. Tilocca, C. Di Valentin and A. Selloni, *J. Phys. Chem. B*, 2005, **109**, 20963.
104 M. A. Henderson, *Surf. Sci.*, 1999, **419**, 174.
105 H. Iddir, S. Öğüt, P. Zapol and N. D. Browning, *Phys. Rev. B*, 2007, **75**, 073203.
106 P. Stone, R. A. Bennett and M. Bowker, *New J. Phys.*, 1999, **1**, 8.
107 R. A. Bennett, P. Stone and M. Bowker, *Faraday Discuss.*, 1999, **114**, 267.
108 R. D. Smith, R. A. Bennett and M. Bowker, *Phys. Rev. B*, 2002, **66**, 035409.
109 R. A. Bennett, *PhysChemComm*, 2003, **3**, 9.
110 K. F. McCarty, *Surf. Sci.*, 2003, **543**, 185.
111 M. Li, W. Hebenstreit and U. Diebold, *Surf. Sci.*, 1998, **414**, L951.
112 M. Li, W. Hebenstreit, U. Diebold, M. A. Henderson and D. R. Jennison, *Faraday Discuss.*, 1999, **114**, 245.
113 M. Li, W. Hebenstreit and U. Diebold, *Phys. Rev. B*, 2000, **61**, 4926.
114 H. Onishi, T. Aruga and Y. Iwasawa, *J. Catal.*, 1994, **146**, 557.
115 M. A. Henderson, *J. Phys. Chem. B*, 1997, **101**, 221.
116 B. E. Hayden, A. King and M. A. Newton, *J. Phys. Chem. B*, 1999, **103**, 203.
117 Z. Chang and G. Thornton, *Surf. Sci.*, 2000, **462**, 68.
118 H. Onishi, K. Fukui and Y. Iwasawa, *Jpn. J. Appl. Phys.*, 1999, **38**, 3830.
119 S. A. Chambers, S. Thevuthasan, Y. J. Kim, G. S. Herman, Z. Wang, E. Tober, R. Ynzunza, J. Morais, C. H. F. Peden, K. Ferris and C. S. Fadley, *Chem. Phys. Lett.*, 1997, **267**, 51.
120 S. Thevuthasan, G. S. Herman, Y. J. Kim, S. A. Chambers, C. H. F. Peden, Z. Wang, R. X. Ynzunza, E. D. Tober, J. Morais and C. F. Fadley, *Surf. Sci.*, 1998, **401**, 261.
121 A. Gutiérrez-Sosa, P. Martínez-Escolano, H. Raza, R. Lindsay, P. L. Wincott and G. Thornton, *Surf. Sci.*, 2001, **471**, 163.
122 D. I. Sayago, M. Polcik, R. Lindsay, R. L. Toomes, J. T. Hoeft, M. Kittel and D. P. Woodruff, *J. Phys. Chem. B*, 2004, **108**, 14316.
123 L.-Q. Wang, K. F. Ferris, A. N. Shultz, D. R. Baer and M. H. Engelhard, *Surf. Sci.*, 1997, **380**, 352.
124 J. Ahdjoudj and C. Minot, *Catal. Lett.*, 1997, **46**, 83.
125 S. P. Bates, G. Kresse and M. J. Gillan, *Surf. Sci.*, 1998, **409**, 336.
126 P. Käckell and K. Terakura, *Appl. Surf. Sci.*, 2000, **166**, 370.
127 P. Käckell and K. Terakura, *Surf. Sci.*, 2000, **461**, 191.
128 M. Bowker, P. Stone, R. Bennett and N. Perkins, *Surf. Sci.*, 2001, **511**, 435.
129 M. Aizawa, Y. Morikawa, Y. Namai, H. Morikawa and Y. Iwasawa, *J. Phys. Chem. B*, 2005, **109**, 18831.
130 R. A. Bennett, P. Stone, R. D. Smith and M. Bowker, *Surf. Sci.*, 2000, **454–456**, 390.
131 H. Onishi, T. Aruga and Y. Iwasawa, *J. Am. Chem. Soc.*, 1993, **115**, 10460.
132 Q. Wang, J. Biener, X.-C. Guo, E. Farfan-Arribas and R. J. Madix, *J. Phys. Chem. B*, 2003, **107**, 11709.
133 Y. Uemura, T. Taniike, M. Tada, Y. Morikawa and Y. Iwasawa, *J. Phys. Chem. C*, 2007, **111**, 16379.
134 Q. Guo, I. Cocks and E. M. Williams, *J. Chem. Phys.*, 1997, **106**, 2924.
135 Q. Guo and E. M. Williams, *Surf. Sci.*, 1999, **433–435**, 322.
136 M. A. Henderson, J. M. White, H. Uetsuka and H. Onishi, *J. Am. Chem. Soc.*, 2003, **125**, 14974.
137 J. M. White, J. Szanyi and M. A. Henderson, *J. Phys. Chem. B*, 2004, **108**, 3592.
138 T. Qiu and M. A. Barteau, *J. Colloid Interface Sci.*, 2006, **303**, 229.
139 A. G. Thomas, W. R. Flavell, C. P. Chatwin, A. R. Kumarasinghe, S. M. Rayner, P. F. Kirkham, D. Tsoutsou, T. K. Johal and S. Patel, *Surf. Sci.*, 2007, **601**, 3828.
140 L. Gundlach, J. Szarko, L. D. Socaciu-Siebert, A. Neubauer, R. Ernstorfer and F. Willig, *Phys. Rev. B*, 2007, **75**, 125320.
141 I. Lyubinetsky, Z. Q. Yu and M. A. Henderson, *J. Phys. Chem. C*, 2007, **111**, 4342.
142 L. Patthey, H. Rensmo, P. Persson, K. Westermark, L. Vayssieres, A. Stashans, Å. Petersson, P. A. Brühwiler, H. Siegbahn, S. Lunell and N. Mårtensson, *J. Chem. Phys.*, 1999, **110**, 5913.
143 M. Odelius, P. Persson and S. Lunell, *Surf. Sci.*, 2003, **529**, 47.
144 A. Sasahara, C. L. Pang and H. Onishi, *J. Phys. Chem. B*, 2006, **110**, 4751.
145 I. D. Cocks, Q. Guo, R. Patel, E. M. Williams, E. Roman and J. L. de Segovia, *Surf. Sci.*, 1997, **377**, 135.
146 E. Soria, I. Colera, E. Roman, E. M. Williams and J. L. de Segovia, *Surf. Sci.*, 2000, **451**, 188.
147 H. Onishi, Y. Yamaguchi, K. Fukui and Y. Iwasawa, *J. Phys. Chem.*, 1996, **100**, 9582.
148 H. Idriss, P. Légare and G. Maire, *Surf. Sci.*, 2002, **515**, 413.
149 J. M. White and M. A. Henderson, *J. Phys. Chem. B*, 2005, **109**, 12417.
150 M. A. Henderson, J. M. White, H. Uetsuka and H. Onishi, *J. Catal.*, 2006, **238**, 153.
151 M. A. Henderson, S. Otero-Tapia and M. E. Castro, *Faraday Discuss.*, 1999, **114**, 313.
152 J. E. Parmeter, X. Jiang and D. W. Goodman, *Surf. Sci.*, 1990, **240**, 85.
153 M. A. Henderson, S. Otero-Tapia and M. E. Castro, *Surf. Sci.*, 1998, **412/413**, 252.
154 R. Sánchez de Armas, J. Oviedo, M. A. San Miguel and J. F. Sanz, *J. Phys. Chem. C*, 2007, **111**, 10023.
155 K. Onda, B. Li, J. Zhao and H. Petek, *Surf. Sci.*, 2005, **593**, 32.
156 B. Li, J. Zhao, K. Onda, K. D. Jordan, J. Yang and H. Petek, *Science*, 2006, **311**, 1436.
157 Z. Zhang, O. Bondarchuk, J. M. White, B. D. Kay and Z. Dohnálek, *J. Am. Chem. Soc.*, 2006, **128**, 4198.
158 E. Farfan-Arribas and R. J. Madix, *Surf. Sci.*, 2003, **544**, 241.
159 O. Bondarchuk, Y. K. Kim, J. M. White, J. Kim, B. D. Kay and Z. Dohnálek, *J. Phys. Chem. C*, 2007, **111**, 11059.
160 E. Farfan-Arribas and R. J. Madix, *J. Phys. Chem. B*, 2002, **106**, 10680.
161 D. Brinkley and T. Engel, *J. Phys. Chem. B*, 2000, **104**, 9836.
162 L. Gamble, L. S. Jung and C. T. Campbell, *Surf. Sci.*, 1996, **348**, 1.
163 Y. K. Kim, B. D. Kay, J. M. White and Z. Dohnálek, *J. Phys. Chem. C*, 2007, **111**, 18236.
164 Z. Zhang, O. Bondarchuk, B. D. Kay, J. M. White and Z. Dohnálek, *J. Phys. Chem. C*, 2007, **111**, 3021.
165 Y. K. Kim, B. D. Kay, J. M. White and Z. Dohnálek, *Catal. Lett.*, 2007, **119**, 1.
166 D. Brinkley and T. Engel, *Surf. Sci.*, 1998, **415**, L1001.
167 D. Brinkley and T. Engel, *J. Phys. Chem. B*, 1998, **102**, 7596.
168 P. M. Jayaweera, E. L. Quah and H. Idriss, *J. Phys. Chem. C*, 2007, **111**, 1764.
169 T. Reztova, C.-H Chang, J. Koresh and H. Idriss, *J. Catal.*, 1999, **185**, 223.
170 B. C. Stipe, M. A. Rezaei and W. Ho, *Science*, 1998, **280**, 1732.
171 L. Leung, C. A. Muryn and G. Thornton, *Surf. Sci.*, 2004, **566–568**, 671.
172 A. Locatelli and E. Bauer, *J. Phys.: Condens. Matter*, 2008, **20**, 093002.
173 F. Schedin, L. Leung and G. Thornton, *J. Appl. Phys.*, 2004, **95**, 7450.